

**Nonlinear Bloch waves in resonantly doped photonic crystals**

Artan Kaso\* and Sajeev John

*Department of Physics, University of Toronto, 60 St. George Street, Toronto, Ontario, Canada M5S 1A7*

(Received 25 June 2006; published 18 October 2006)

We demonstrate the existence of self-consistent Bloch modes in resonant nonlinear photonic crystals with a complex, intensity-dependent, and frequency-dependent dielectric function. Such a dielectric response may arise by “doping” the photonic crystal with resonant quantum dots, atomic impurities, or other two-level light emitters. These exact solutions of the nonlinear electromagnetic wave equation exhibit Bloch periodicity and describe fundamental eigenmodes of an active photonic crystal under incoherent pumping. In a simple model two-dimensional photonic crystal, doped with active two-level atoms, the optical field intensity of these waves shows a laserlike threshold behavior with pumping. This appears to be a universal property of active, nonlinear photonic crystals and photonic band gap materials, arising from multidirectional distributed feedback. We describe an iterative technique for computing the detailed properties of these exact, self-consistent nonlinear waves in strongly scattering photonic crystal architectures with regions of gain and loss.

DOI: [10.1103/PhysRevE.74.046611](https://doi.org/10.1103/PhysRevE.74.046611)

PACS number(s): 42.70.Qs, 42.55.Tv

**I. INTRODUCTION**

Photonic band gap (PBG) materials [1,2] are artificial periodic dielectrics that enable the localization, trapping, and confinement of light [1,3] on the wavelength scale. In the absence of disorder and for linear dielectric constants that are typically real, positive, and frequency independent, the solutions to Maxwell’s equations within the photonic crystal (PC) satisfy Bloch’s theorem [4]. These Bloch modes can be efficiently represented as a plane wave expansion [5]. Optimized photonic band gap materials have a solid dielectric backbone with typical volume fraction of less than 25%. Important phenomena arise when the photonic crystal void regions are infiltrated with active, nonlinear materials, or when the PC backbone is doped with resonant nonlinear atoms or quantum dots [6–11]. These phenomena include laser activity and nonlinear switching effects [12–20]. In these situations, computational methods are required to quantitatively describe the effects of complex, frequency dependent, and nonlinear dielectric response in a strongly scattering periodic medium. This is especially important when nonlinear effects modify the underlying photonic band structure and electromagnetic wave equations. The resulting solutions of the nonlinear wave equation must be self-consistently determined.

In this paper we introduce a self-consistent iterative technique to describe electromagnetic modes in a strongly scattering periodic microstructure with resonant nonlinearities and complex frequency-dependent dielectric functions. In this medium, the imaginary part of the nonlinear dielectric function can be either positive or negative, corresponding to absorption or gain in specific regions of the PC. The PC can also be uniformly pumped (electrically or optically) by an external power source. Under suitable pumping conditions, we demonstrate the existence of exact solutions of the nonlinear wave equation, in such a medium, satisfying Bloch’s theorem. These nonlinear waves typically require a threshold pumping condition in order to overcome absorption losses.

They correspond to a specific number of “photons” (field energy) per unit cell of the PC for a specific value of the pump and the complex nonlinear dielectric profile. If the photon number per unit cell falls below the required value, the eigenfrequency of the nonlinear wave acquires an imaginary part leading to temporal amplification of the field amplitude. Self-consistent, steady state solutions occur only for a specific wave amplitude. This behavior is characteristic of laserlike field oscillations that have been observed at photonic band edges [20]. At a photonic band edge, slow group velocity [21,22] and multidirectional distributed feedback [20] contribute to self-consistent nonlinear oscillation in the presence of loss. We find, very strikingly, that self-consistent, steady state nonlinear Bloch wave solutions can occur at any point in the photonic band structure and are not restricted to photonic band edges.

We illustrate the nature of nonlinear Bloch waves in three physical systems of resonantly doped two-dimensional (2D) photonic crystals with small overall damping coefficients. In the first we consider a silicon PC with an added gain region consisting of erbium-doped silica. In this case the dopant atoms provide only a very weak perturbation to the background frequency-independent dielectric function of the silica-silicon host material. Here the number of photons per unit cell in the self-consistent nonlinear Bloch waves remains relatively small for pumping levels just above threshold for steady state oscillation. The second and third illustrations consider much larger nonlinear perturbations caused by resonant doping. In these cases, we study a dense coating of colloidal quantum dots on the interior surfaces of a silicon PC containing a square lattice of holes. We consider both a thin coating and a thick coating of close packed PbS quantum dots each capped by a thin polymer shell. In these cases, the nonlinear Bloch waves have considerably larger amplitude than the case of erbium-doped silica and self-consistent steady state oscillation survives in the presence of larger background losses.

In addition to the physical systems described above, our methodology for describing complex, nonlinear photonic crystals is relevant to a variety of other problems of current interest. For example, distributed feedback lasers [23] con-

\*Electronic address: [akaso@physics.utoronto.ca](mailto:akaso@physics.utoronto.ca)

structed from relatively weak scattering Bragg gratings are described by an approximate coupled mode analysis [24]. This description is accurate in the limit of a very small 1D photonic stop gap. Our exact method can treat very strongly scattering periodic microstructures in 1D, 2D, and 3D containing high or low gain concentrations. Our nonlinear Bloch wave analysis provides a quantitative and predictive tool for the characteristics of future lasers based on strongly scattering PBG materials. Recently, optical gain and stimulated emission have been reported in periodic nanopatterned crystalline silicon [12]. Here lasing is attributed to electron-hole direct recombination centers on the interior surfaces of the nanopatterned silicon. The question of efficient silicon based lasers is of enormous technological importance. In a silicon PBG material (with patterning on the larger scale of roughly 600 nm) distributed feedback effects may lead to nonlinear Bloch waves of the type discussed in this paper. A third possible realization of nonlinear Bloch waves is in electrically pumped metallic photonic crystal filaments. In tungsten-based filaments, fabricated in a woodpile PBG architecture [25], it has been reported [26,27] that thermal light emission exhibits characteristics very distinct from a standard blackbody radiator. Peaks in thermal light emission have been observed [28] at frequencies corresponding to structural features of the underlying photonic crystal. In the case of strong electrical pumping, light emission intensity at these frequencies exceeds that of a blackbody at roughly the same temperature. Unlike previous examples, where the light emitters are concentrated in a narrow frequency range, the metallic photonic crystal filament can be modeled [29] using a very broad distribution of two-level emitters. This is an active nonlinear medium with a complex frequency-dependent dielectric function. In this case, the emergence of nonlinear Bloch waves at particular frequencies may provide a basis for enhanced light emission from the filament.

Our iterative method for obtaining exact, self-consistent nonlinear modes in strongly scattering PC's supercedes earlier attempts to describe photonic band structure in frequency-dependent dielectrics. In 2D PC's with a simple analytical expression for the frequency-dependent dielectric function, the finite-difference time domain method and other specialized methods have proved useful in obtaining linear band structure [30–36]. More generally for 3D PC's and completely general forms of the frequency-dependent dielectric function, the so-called “cutting surface method” (CSM) was introduced [37]. However, neither the CSM nor the preceding approaches are capable of describing active, nonlinear photonic crystals with a complex dielectric constant.

In Sec. II of this paper we introduce the three specific illustrative models to which we apply our self-consistent iterative approach to nonlinear photonic band structure. Each of these systems exhibits nonlinear Bloch waves for suitable pumping. In Sec. III of this paper we establish the nonlinear integral equation for the self-consistent Bloch modes of the doped PC and the Green's function kernel of the backbone photonic crystal (BPC). In Sec. IV A we provide diagnostics for our integral equation method by applying it to the simple situation in which one of the dielectric constituents of the BPC is trivially “doped” with an additional dielectric that exhibits purely linear, frequency-independent optical re-

sponse. In Sec. IV B we apply our method to the case of a dopant dielectric exhibiting a real and frequency-dependent susceptibility. In this case, we demonstrate that our iterative method based on the integral equation formulation more efficiently recaptures the results obtained with established techniques such as the CSM [37]. If the susceptibility of the dopant atoms is complex, frequencies for the field inside the PC may also be complex. Such modes either grow or decay exponentially with time. The rate of decay or growth is set by the photon density and a pump parameter,  $\rho$ , both of which enter the nonlinear optical susceptibility of the atomic system. In the case of electrically insulating materials, this pumping may arise from an external incoherent light source that illuminates the volume of the photonic crystal. In the case of electrically conducting photonic crystals the parameter,  $\rho$ , may be related to electrical pumping. In either case, we introduce a small damping (positive imaginary part of the background dielectric constant) over and above the resonant susceptibility. The combination of pumping and damping enables steady state, self-consistent Bloch modes to emerge. In Sec. V we observe how the self-consistent Bloch mode amplitude depends on the incoherent pumping rate for the case of homogeneously broadened dopant atoms, when only a single mode within the composite PC is spontaneously excited. In this situation we identify the occurrence of a nonlinear eigenmode of the photonic crystal with Bloch-mode characteristics. As a function of incoherent pumping, the self-consistent amplitude of this periodic nonlinear oscillation exhibits characteristics of a laser mode.

## II. MODELS OF RESONANT NONLINEAR PHOTONIC CRYSTALS

Radiation relaxation of an excited two-level quantum system in the electric dipole approximation depends on two factors. The first is the matrix element for the electric dipole transition between the excited and the relaxed state of the system and the second is the density of radiation modes through which this radiation can escape. The density of radiation modes can be engineered with the help of PBG materials. Modified properties for electromagnetic modes in a PC are expected if resonant systems (atoms, quantum dots, quantum wells, etc.) within the PC are subjected to local electromagnetic density of states modification [20,38–40]. In this paper we introduce a self-consistent field method that can quantitatively describe extended Bloch modes in the presence of a variety of such phenomena. To illustrate our computational method we consider three situations.

(a) A square lattice of cylindrical silicon (Si) rods where the space between the rods is filled with glass ( $\text{SiO}_2$ ) of dielectric constant  $\epsilon_b=2.1$ . The lattice constant is  $a$ , the radius of the rods is  $r=0.3a$ , and their dielectric constant  $\epsilon_a=12.1$ . The glass is uniformly doped with erbium triply ionized atoms ( $\text{Er}^{3+}$ ) which under a suitable pumping represent our radiative system. A schematic view of the unit cell of this PC is presented in Fig. 1(a).

(b) A square lattice of cylindrical air pores etched in silicon matrix (Si) of dielectric constant  $\epsilon_b=12.1$ . The lattice constant is  $a$ , the radius of the pores is  $r=0.45a$ , and their

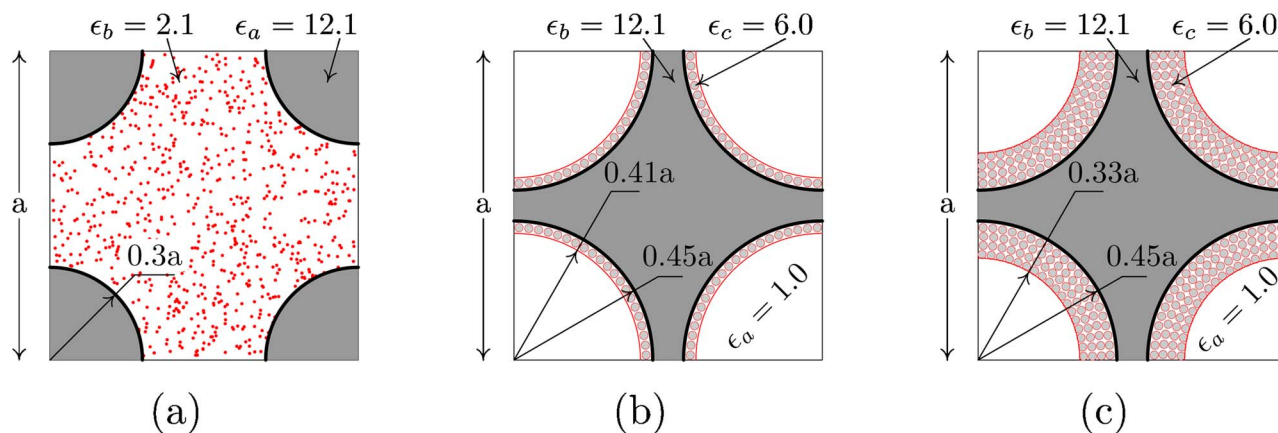


FIG. 1. (Color online) (a) Unit cell of the square lattice of silicon (Si,  $\epsilon_a=12.1$ ) cylindrical rods (radius  $r=0.3a$ ) in glass matrix ( $\text{SiO}_2$ ,  $\epsilon_b=2.1$ ). Dots (red online) represent the uniform distribution (random) of the dopant atoms within the glass component. (b) Unit cell of the square lattice of air cylindrical pores (radius  $r=0.45a$ ,  $\epsilon_a=1.0$ ) etched in silicon matrix (Si,  $\epsilon_b=12.1$ ). Light (red online) regions represent the coating of the silicon matrix with close packed colloidal quantum dots. The thickness of the coated shell is  $0.04a$ . The average, frequency-independent dielectric constant of the coating is  $\epsilon_c=6.0$ . (c) The same as (b) but now the coating has a thickness  $0.12a$ .

dielectric constant  $\epsilon_a=1.0$ . The inner surface of air pores is coated with close packed colloidal quantum dots. The thickness of the coating shell is  $\delta=0.04a$ . Quantum dots under a suitable pumping represent our active medium. A schematic view of the unit cell of this PC is presented in Fig. 1(b).

(c) The photonic structure is the same as the one described in (b) but now the radiative coating brings a substantial contribution to the overall photonic band structure, due to a larger coating thickness and the higher number of resonant quantum dots. In the following, for the sake of the argument, we focus on the case (a). Numerical results for all three cases are presented in Sec. VI.

We refer to the part of the PC consisting of silicon rods and glass matrix as the BPC. We assume that the dopant atoms are uniformly distributed in the glass regions with the same average spatial periodicity as the host BPC. If a macroscopic number of dopant atoms is considered (e.g.,  $N_T \sim 10^{19} \text{ cm}^{-3}$ , where  $N_T$  is the volumetric density of the dopant atoms) we may expect that their presence will influence both the frequency distribution and the nature of the electromagnetic eigenmodes in the PC. To numerically investigate these effects, we introduce an iterative self-consistent optical field method based on an integral equation formulation of Maxwell's equation with a nonlinear dielectric. In this integral equation, the influence of the BPC is evaluated through a Green's function kernel (propagator) and is separated from the influence of the dopant atoms. The active, nonlinear dielectric component, on the other hand, appears as a self-consistent potential in the integral equation. At each iterative step, the normalized eigenmodes and (real) frequencies are updated by the results of the previous iteration until the output eigenfrequency coincides with the input frequency appearing in the self-consistent potential.

The convergence of this iterative algorithm is analogous to the Hartree-Fock method in solid state physics. Unlike the Hartree-Fock solution, in many electron systems, the self-consistent Bloch-mode solution that we obtain is an exact solution of the nonlinear wave equation in the photonic crystal. The electromagnetic eigenmodes of the BPC constitute

the “unperturbed” system while the periodic distribution of the dopant atoms is the “perturbation.” At each iteration, the influence of the perturbation from the previous iteration is used to update the normal modes of the system. On the other hand, the perturbation itself is chosen self-consistently by adjusting the nonlinear dielectric response to correspond to a specific number of photons per unit cell of the PC. Finally the number of photons per unit cell must be adjusted to yield eigenmodes with a real frequency that neither grow nor decay exponentially. We do not impose any limitation on the strength of the perturbation except for the strict requirement that the real part of the total dielectric constant of the combined system (BPC plus dopant atoms) be positive at all frequencies. This restriction is not fundamental to the underlying physics, rather it is respected in order to achieve rapid convergence. While the language used is the same as that used in the quantum perturbation theory, the method used is not an approximate one. The strength of the perturbation in our method simply alters the computational time required to reach the exact solution.

The effect of dopant atoms on the radiation modes is a frequency shift of the modes able to freely propagate into the doped PC. Dopant atoms respond to the local field by scattering and absorbing or amplifying it. This response is captured by the (ensemble averaged, nonlinear) susceptibility. Two important parameters enter the susceptibility:  $T_1$ , the depopulation time of the excited level and  $T_2$ , the dephasing time of the electric dipole moment of the excited atomic system. For simplicity we consider only the modes with electric field polarized perpendicular to the plane of the 2D BPC (TM modes). In our model we make two further assumptions for the sake of computational simplicity.

(1) The resonance frequency of the dopant atoms is the same for all dopant atoms (crystal-field Stark shift of the resonant frequency leading to inhomogeneous line broadening is ignored). This resonance frequency is independent of the strength of the radiation field established in PC. These assumptions are not required for the application of our method of analysis. They provide computational simplicity for the purpose of illustration.

(2)  $T_1$  and  $T_2$  are assumed to be independent of frequency and applied fields. In general, the rate of population relaxation,  $T_1^{-1}$ , is the sum of contributions from radiative and nonradiative processes. In material systems where luminescence is observed, the rate of radiative decay,  $T_{1,\text{rad}}^{-1}$ , is significant compared to the rate of nonradiative decay,  $T_{1,\text{nonrad}}^{-1}$ . In photonic crystals with a PBG or even a significant suppression in the 3D electromagnetic density of states (DOS),  $T_{1,\text{rad}}$  may vary with frequency according to the frequency dependence of the DOS [6]. When the frequency variation of the DOS is sufficiently rapid, non-Markovian memory effects may appear in the radiative dynamics and a more elaborate description is required [41]. Within a complete PBG  $T_{1,\text{rad}}^{-1}$  may vanish [38,42]. However, for a collection of proximal light emitters, depopulation of the excited state of any given emitter may occur through the higher order radiative process of resonance dipole-dipole interaction [40]. If transfer of energy (sometimes called Forster energy transfer) exceeds  $T_{1,\text{nonrad}}^{-1}$ , then entirely new forms of resonant nonlinear optical response may arise [43–45]. While our iterative technique for evaluating self-consistent Bloch modes can describe the dramatic effects of a 3D PBG, we choose to illustrate our method here using the simpler context of 2D photonic crystals. In 2D PCs, the local and total 3D electromagnetic DOS remains similar to the DOS of free space [46]. In this case we assume frequency and intensity independent  $T_1$  and  $T_2$ . Soft collisions (e.g., elastic phonon-dopant atom collisions) are responsible for  $T_2$ , and we expect them to remain unaffected by the presence of the PC.

In the event of the population inversion of the dopant atoms, resonant electromagnetic waves propagating through the PC may experience gain. The amplitude of the field is limited due to power broadening of the atomic resonance and eventual gain saturation [47,48]. In our method, power broadening is iteratively fed back to the dielectric constant of the PC through the nonlinear, intensity-dependent susceptibility of the dopant atoms. When the photon density is readjusted to yield a purely real output frequency, self-consistent extended Bloch modes appear. We refer to these self-consistent Bloch modes as “nonlinear eigenmodes” of the active PC and we refer to our method as the nonlinear eigenmodes method.

### III. PHOTON PROPAGATOR FOR THE PASSIVE BACKBONE PHOTONIC CRYSTAL

In this section, we introduce the Green function of the BPC, that describes the frequency-independent part (BPC) of the system separately from the frequency- and field-dependent perturbation. This separation leads to computational efficiency by limiting the iterative, self-consistent field calculation to the frequency-dependent and nonlinear part of the material. In this approach we obtain an exact solution to the band structure of complex, nonlinear, frequency-dependent dielectrics in an iterative way.

In a two-dimensional photonic crystal, Maxwell’s equations for the  $E$ -polarized (electric field vector everywhere perpendicular to the plane of periodicity) field in the presence of the dopant atoms reduce to the nonlinear wave equation

$$\nabla^2 E_\omega(\vec{r}) + \frac{\omega^2}{c^2} [\epsilon(\vec{r}) + 4\pi\chi_\omega(\vec{r})] E_\omega(\vec{r}) = 0. \quad (1)$$

Here  $\epsilon(\vec{r})$  is the spatially dependent, frequency-independent, *real* dielectric constant of the BPC, and  $4\pi\chi_\omega(\vec{r})$  represents the complex, nonlinear, and frequency-dependent susceptibility of the dopant atoms. The eigenfunctions of the BPC satisfy

$$\nabla^2 \psi_{\vec{k},l}(\vec{r}) + \frac{\omega_{\vec{k},l}^2}{c^2} \epsilon(\vec{r}) \psi_{\vec{k},l}(\vec{r}) \equiv 0, \quad (2)$$

where  $\vec{k}$  is a *real* vector of reciprocal space in the first Brillouin zone,  $l$  is a band index label, and  $\omega_{\vec{k},l}$  is the dispersion relation for the  $l$ th band of the BPC. By construction (Appendix A) the eigenmodes of the BPC are Bloch states and can be written as

$$\psi_{\vec{k},l}(\vec{r}) = e^{i\vec{k}\vec{r}} u_{\vec{k},l}(\vec{r}) \equiv e^{i\vec{k}\vec{r}} \sum_{\vec{G}} \tilde{u}_{\vec{k},l}(\vec{G}) e^{i\vec{G}\vec{r}}. \quad (3)$$

Here, the summation is over reciprocal lattice vectors  $\vec{G}$ , the function  $u_{\vec{k},l}(\vec{r})$  has the periodicity of direct lattice, and  $e^{i\vec{k}\vec{r}}$  is the Bloch phase. Since we assume  $\epsilon(\vec{r})$  real, Eq. (2) is the eigenvalue problem for a self-adjoint operator. It follows that

$$\frac{1}{V} \int_V d^2r \psi_{\vec{q},n}^*(\vec{r}) \epsilon(\vec{r}) \psi_{\vec{k},l}(\vec{r}) = \delta_{\vec{q},\vec{k}} \delta_{n,l} \quad (4)$$

upon normalization of the eigenvectors (Appendix A). In Eq. (4) the integration is over the whole two-dimensional volume  $V$  of the photonic crystal [49].

We may represent a general electric field  $E_\omega(\vec{r})$  at point  $\vec{r}$  as a superposition of the complete set of Bloch fields  $\psi_{\vec{k},l}(\vec{r})$  (all eigenvectors of BPC). The coefficients of this superposition are complex numbers,  $f_{\vec{k},l}$

$$E_\omega(\vec{r}) = \sum_{\vec{k},l} f_{\vec{k},l} \psi_{\vec{k},l}(\vec{r}). \quad (5)$$

Here, the wave vector summation extends over the first Brillouin zone of the PC and  $l$  moves over all bands. Inserting Eq. (5) into Eq. (1) and using Eq. (2) we obtain

$$\sum_{\vec{k},l} f_{\vec{k},l} (\omega_{\vec{k},l}^2 - \omega^2) \epsilon(\vec{r}) \psi_{\vec{k},l}(\vec{r}) = \omega^2 4\pi\chi_\omega(\vec{r}) E_\omega(\vec{r}). \quad (6)$$

Multiplying both sides of Eq. (6) by  $\psi_{\vec{q},n}^*(\vec{r})$  and integrating over the whole photonic crystal and using Eq. (4) we obtain

$$f_{\vec{q},n} = \frac{1}{V} \int_V d^2r' \frac{\psi_{\vec{q},n}^*(\vec{r}')}{\Delta_{\vec{q},n}} 4\pi\chi_\omega(\vec{r}') E_\omega(\vec{r}'), \quad (7a)$$

where

$$\Delta_{\vec{q},n} \equiv \frac{\omega_{\vec{q},n}^2}{\omega^2} - 1. \quad (7b)$$

Multiplying both sides of Eq. (7b) by  $\psi_{\vec{q},n}(\vec{r})$  and summing over  $\{\vec{q},n\}$  we obtain the integral equation

$$E_\omega(\vec{r}) = \frac{1}{V} \int_V d^2r' G_\omega(\vec{r}, \vec{r}') 4\pi\chi_\omega(\vec{r}') E_\omega(\vec{r}'), \quad (8)$$

where

$$G_\omega(\vec{r}, \vec{r}') = \sum_{\vec{q}, l} \frac{\psi_{\vec{q}, l}(\vec{r}) \psi_{\vec{q}, l}^*(\vec{r}')}{\Delta_{\vec{q}, l}} \quad (9)$$

is the Green function of the BPC [50]. This BPC photon propagator plays a role analogous to the “free-particle propagator” in quantum scattering theory. Equation (8) is the analog of the Lippmann-Schwinger integral equation in quantum scattering theory [51], where  $4\pi\chi_\omega(\vec{r}')$  plays the role of a scattering potential.

#### IV. PASSIVELY DOPED PHOTONIC CRYSTALS: LINEAR EIGENMODES

An instructive application of our integral equation method of electromagnetic band structure is in the case that the perturbation  $4\pi\chi_\omega(\vec{r})$  consists of the same material as the BPC. This can be solved also by the PWE method. In Sec. IV A, we provide a diagnostic comparison of the efficiency and accuracy of our integral equation method using this simple illustration. In Sec. IV B, we provide a second diagnostic comparison to the previously introduced cutting surface method [37] for the case of linear but frequency-dependent dielectric perturbation.

##### A. Linear response to nonresonant perturbation

Consider a perturbation to the BPC consisting of nonresonant atoms that form a lattice with the periodicity of the BPC. We can write

$$\chi(\vec{r}) = \sum_{\vec{R}} \bar{\chi}(\vec{r} + \vec{R}), \quad (10)$$

with  $\vec{R}$ , a translation vector of the BPC and  $\bar{\chi}(\vec{r})$ , a function different from zero only within the primitive cell of the BPC. We seek solutions  $E_\omega(\vec{r})$  of Eq. (1) that satisfy the Bloch periodicity

$$E_\omega(\vec{r} + \vec{R}) = e^{i\vec{q}\cdot\vec{R}} E_\omega(\vec{r}), \quad (11)$$

where  $\vec{q}$  is a Bloch vector from the first Brillouin zone of the lattice. Using Eqs. (8), (10), and (11) we can write

$$E_\omega(\vec{r}) = \frac{1}{V_0} \int_{V_0} d^2r' \mathcal{G}_{\omega, \vec{q}}(\vec{r}, \vec{r}') 4\pi\bar{\chi}(\vec{r}') E_\omega(\vec{r}'), \quad (12a)$$

where

$$\begin{aligned} \mathcal{G}_{\omega, \vec{q}}(\vec{r}, \vec{r}') &\equiv \frac{1}{N} \sum_{\vec{R}'} G_\omega(\vec{r} + \vec{R}, \vec{r}' + \vec{R}') e^{i\vec{q}(\vec{R}' - \vec{R})} \\ &= \sum_l \frac{\psi_{\vec{q}, l}^*(\vec{r}') \psi_{\vec{q}, l}(\vec{r})}{\Delta_{\vec{q}, l}}. \end{aligned} \quad (12b)$$

Here,  $N$  is the number of sites of the lattice and  $V_0 = V/N$  is

the 2D volume of the unit cell of the 2D lattice. In deriving Eq. (12a) we used [4]

$$\sum_{\vec{R}'} e^{i(\vec{q} - \vec{k})(\vec{R}' - \vec{R})} = N \delta_{\vec{q}, \vec{k}}.$$

We now expand the Bloch fields in the basis of eigenfunctions of the BPC by using Eq. (5). Inserting this expansion into Eq. (12a), multiplying both sides of the resulting equation by  $\psi_{\vec{k}_2, l_2}^*(\vec{r}) \epsilon(\vec{r})$ , integrating over the whole photonic crystal, and using the orthogonality relation Eq. (4), we obtain

$$f_{\vec{k}_2, l_2} = \delta_{\vec{q}, \vec{k}_2} \frac{1}{\Delta_{\vec{q}, l_2} \bar{\Delta}_{\vec{q}, l_2, \vec{k}_1, l_1}} \sum \mathcal{X}_{\vec{q}, l_2; \vec{k}_1, l_1} f_{\vec{k}_1, l_1}, \quad (13a)$$

where

$$\mathcal{X}_{\vec{q}, l_2; \vec{k}_1, l_1} \equiv \frac{1}{V_0} \int_{V_0} d^2r' \psi_{\vec{q}, l_2}^*(\vec{r}) 4\pi\bar{\chi}(\vec{r}) \psi_{\vec{k}_1, l_1}(\vec{r}). \quad (13b)$$

Equation (13a) reveals that  $f_{\vec{k}_2, l_2} \equiv 0, \forall l_2$  if  $\vec{k}_2 \neq \vec{q}$ . Consequently, the summation over  $\vec{k}_1$  can be reduced to the single term  $\vec{k}_1 = \vec{q}$ . This demonstrates that any perturbation, with the same periodicity as the BPC, couples only those eigenmodes from different bands of the BPC with the same Bloch vector  $\vec{q}$ . In our search for self-consistent Bloch modes, we consider only polarization patterns that preserve the translational symmetry of the BPC. The eigenmodes of this active photonic crystal corresponding to the Bloch vector  $\vec{q}$  can, therefore, be represented as a superposition of Bloch modes of the BPC with the same  $\vec{q}$ .

Equation (13a) can be solved as an eigenvalue equation for the eigenfrequencies  $\omega$  of the perturbed BPC. Symmetrizing Eq. (13a) by introducing the variable  $h_{\vec{q}, l} \equiv (\omega_{\vec{q}, l}/c) f_{\vec{q}, l}$ , we obtain

$$\sum_{l_1} B_{\vec{q}}(l_2; l_1) h_{\vec{q}, l_1} = \frac{c^2}{\omega^2} h_{\vec{q}, l_2}, \quad (14a)$$

where

$$B_{\vec{q}}(l_2; l_1) \equiv \frac{c^2}{\omega_{\vec{q}, l_2} \omega_{\vec{q}, l_1}} (\delta_{l_2, l_1} + \mathcal{X}_{\vec{q}, l_2; \vec{q}, l_1}). \quad (14b)$$

The matrix  $B_{\vec{q}}(l_2; l_1)$  is Hermitian if the function  $\bar{\chi}(\vec{r})$  is real. Equation (14a) can be rewritten in the form of a standard eigenvalue Hermitian equation

$$\sum_{l_2} B_{\vec{q}}^{-1}(l_3; l_2) h_{\vec{q}, l_2} = \frac{\omega^2}{c^2} h_{\vec{q}, l_3}. \quad (15)$$

Clearly, Bloch eigenmodes of the BPC, with a given Bloch vector  $\vec{q}$  but different band indices, are intermixed by the perturbation  $4\pi\chi(\vec{r})$  with the same BPC periodicity. The new Bloch eigenmodes for the complete PC have different frequencies from the eigenfrequencies of the BPC. The new frequencies  $\omega$  are the eigenmodes of Eq. (15) with the corresponding set of coefficients  $\{h_{\vec{q}, l}\}$  needed to build the new Bloch fields  $E_{\vec{q}}(\vec{r}, \omega)$  as a superposition of the eigenmodes  $\psi_{\vec{q}, l}(\vec{r})$  of the BPC.

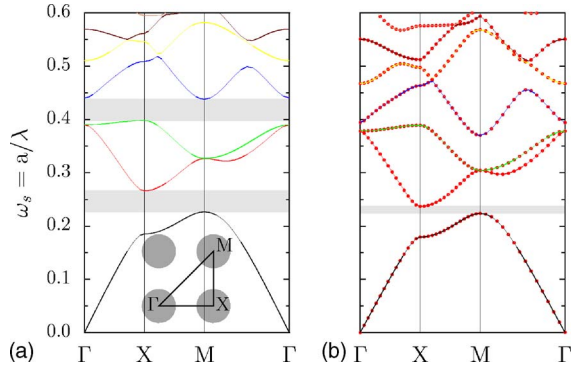


FIG. 2. (Color online) (a) Photonic band structure of the square lattice of silicon cylindrical rods ( $r=0.3a$ ,  $\epsilon_a=12.1$ ) in a glass matrix ( $\epsilon_b=2.1$ ). (b) The structure of (a) but now the glass matrix is modified by the addition of a susceptibility  $4\pi\bar{\chi}(\vec{r})=\tilde{\epsilon}_b-\epsilon_b$ , with  $\tilde{\epsilon}_b=3.3$ . Solid lines represent an exact calculation of the new structure using the PWE method with 3000 plane waves. The dots represent the calculation using our method. 156 first Bloch modes of the BPC are considered coupled from the perturbation.

As a diagnostic of the accuracy of the method described so far, we calculate the photonic band structure of the BPC described in Sec. II consisting of a square lattice of silicon rods ( $\epsilon_a=12.1$ ) embedded in a glass matrix ( $\epsilon_b=2.1$ ), where, instead of doping the glass matrix with resonant atoms, we simply substitute the glass with another passive medium with dielectric constant  $\tilde{\epsilon}_b=3.3$ . In this simple but instructive illustration, the final PC band structure emerges from a single iteration since the perturbation is neither frequency nor intensity dependent. The perturbation in this illustration is

$$4\pi\bar{\chi}(\vec{r}) = \begin{cases} \tilde{\epsilon}_b - \epsilon_b, & \text{in glass region,} \\ 0, & \text{otherwise.} \end{cases} \quad (16)$$

It is instructive to compare the results of the coupled mode (CM) integral equation method [Eqs.(12)–(15)] using the BPC photon propagator Eq. (9) with direct application of the PWE method to the modified structure. The comparison is shown in Fig. 2. Here we introduce the scaled frequency  $\omega_s = \omega c / 2\pi a = a/\lambda$ , where  $a$  is the lattice constant and  $\lambda \equiv 2\pi c/\omega$  is the vacuum wavelength.

TABLE I. Band structure of the square lattice of silicon cylindrical rods ( $r=0.3a$ ,  $\epsilon_a=12.1$ ) in a glass matrix ( $\epsilon_b=2.1$ ), where the glass matrix is “perturbed” by the addition of a susceptibility  $4\pi\bar{\chi}(\vec{r})=\tilde{\epsilon}_b-\epsilon_b$ , with  $\tilde{\epsilon}_b=3.3$ , is calculated using our coupled mode (CM) method. Shown in the table are the eigenfrequencies of bands 2, 3, 4, and 10 at the X point when a number of 10, 26, 56, 156, and 301 modes of the BPC are considered coupled from the perturbation. The frequencies of the same bands at the X point, for the square lattice of silicon cylindrical rods ( $r=0.3a$ ,  $\epsilon_a=12.1$ ) in a matrix of a dielectric with constant  $\epsilon_b=3.3$ , calculated using the PWE method with 3000 plane waves, are shown for comparison.

Bands at the X point	PWE 3000	CM 10	CM 26	CM 56	CM 156	CM 301
2	0.237 084	0.237 156	0.237 094	0.237 089	0.237 084	0.237 084
3	0.389 059	0.389 527	0.389 142	0.389 084	0.389 063	0.389 061
4	0.463 572	0.463 972	0.463 623	0.463 599	0.463 577	0.463 574
10	0.735 350	0.739 091	0.735 919	0.735 448	0.735 361	0.735 353

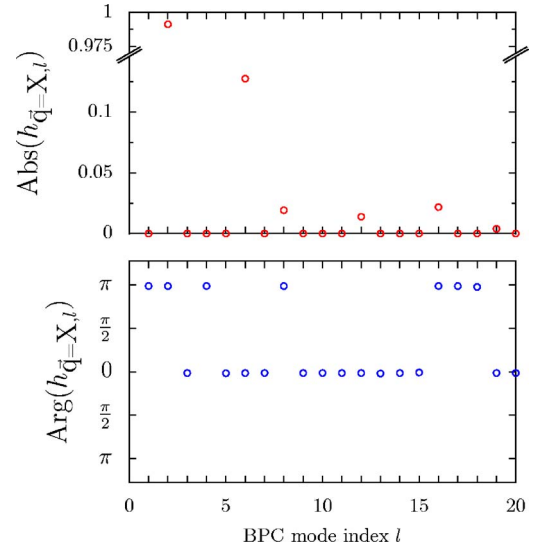


FIG. 3. (Color online) 156 first Bloch modes of the BPC [see Fig. 2(a)] are coupled from the perturbation [read Fig. 2(b) caption]. The coupling coefficients are  $h_{\vec{q},l} \equiv \omega_{\vec{q},l} / c f_{\vec{q},l}$ . Only the first 20 of the coupling coefficients  $\{h_{\vec{q},l}\}$  for  $\vec{q}=X$  point and the second photonic band of the doped BPC are shown.

As expected, the photonic band structure is shifted by the dielectric modification described by Eq. (16). For example, the frequency of the second band at the X point for the BPC is  $\omega_s=0.266$ , whereas in the BPC modified according to Eq. (16), it becomes  $\omega_s=0.237$ . The coupling coefficients  $\{h_{\vec{q},l}\}$  describing the new Bloch mode of the second band at the X point are shown in Fig. 3. Clearly, the main contributions to the modified Bloch mode (X point, second band) come from the eigenmodes of the second and sixth bands of the BPC at the same wave vector. These main contributions are  $\pi$  out of phase.

Most significantly, as shown in Table I, by using only a small number of basis modes of the BPC we are able to accurately recapture the photonic band structure of the perturbed crystal. In contrast, 3000 plane waves were required to represent the eigenmodes of the perturbed photonic crystal to the same level of accuracy. Using a basis of BPC Bloch modes rather than plane waves, the dimension of the matrix

eigenvalue problem for the modified PC is typically reduced by two orders of magnitude.

In treating materials with nonlinear, frequency-dependent, and complex dielectric functions, foreknowledge of the BPC Bloch modes provides a highly efficient starting point for self-consistent and iterative determination of optical modes in active, nonlinear “dopant” materials. The separation of the band structure calculation of the BPC and dopant perturbation provides even more profound computational efficiency in case of 3D, nonlinear, photonic crystals.

### B. Linear, frequency-dependent response of resonant dopant atoms

A more interesting diagnostic of our integral equation formulation arises if the function  $\bar{\chi}(\vec{r})$  appearing in Eq. (13b) is real and linear but frequency dependent. As an illustration, we consider the susceptibility function with a resonance at the (scaled) dimensionless frequency  $\omega_{0s} = \omega_0 a / 2\pi c$

$$\bar{\chi}(\vec{r}, \omega_s) = g_0 \frac{(\omega_s - \omega_{0s})\tau}{1 + (\omega_s - \omega_{0s})^2 \tau^2} \theta_a(\vec{r}), \quad (17a)$$

where the step function

$$\theta_a(\vec{r}) = \begin{cases} 0, & \text{for } \vec{r} \text{ within the rods,} \\ 1, & \text{otherwise.} \end{cases} \quad (17b)$$

Here,  $\omega_s \equiv \omega a / 2\pi c$  where  $\omega$  is the frequency of light and  $\tau \equiv 2\pi c T / a$  where  $T$  is the atomic decay time. In this model, the eigenfrequency  $\omega$ , appearing in Eq. (15) also appears nonlinearly in the scattering potential itself. As such, the eigenvalue problem is not solved unless the frequencies on the left hand side and right hand side of Eq. (15) coincide.

This nonlinear eigenvalue problem is amenable to solution using a self-consistent, iterative procedure. To illustrate the convergence of the iteration we consider the eigenmode having a particular Bloch vector and band index  $(\vec{q}, n)$ , for example  $(\vec{q}=X, n=2)$ . We start the iteration by computing the frequency of the Bloch mode of the BPC [in the absence of frequency dependent  $\bar{\chi}(\vec{r}, \omega_s)$  in Eq. (13b)] at this  $(\vec{q}, n)$  position in the band structure. This provides an initial output eigenfrequency  $\omega_s$  that we insert in the perturbation  $\bar{\chi}(\vec{r}, \omega_s)$  given by Eq. (17a), to begin the iterative process. This value of  $\bar{\chi}(\vec{r}, \omega_s)$  is used in Eq. (13b) to produce an updated eigenfrequency according to Eq. (15) of the revised Bloch mode for the same  $(\vec{q}, n)$  position. This process is iterated until there is almost no further change between the output eigenfrequency in Eq. (15) and the input frequency (from the previous iteration) used in  $\bar{\chi}$ . More specifically, the criterion  $|\omega_{s,m+1} - \omega_{s,m}| < 10^{-4}$  (where  $m$  denotes the  $m$ th iteration step) is employed to end the iteration procedure. The iteration procedure is repeated separately for every point  $(\vec{q}, n)$  of the photonic band structure of the BPC, until a complete “self-consistent” band structure is obtained. This procedure converges very rapidly in most cases, as illustrated in Figs. 4(b) and 4(c).

To check the validity of this self-consistent approach we compare our results with those obtained by the previously introduced CSM [37]. The CSM is an alternative method for

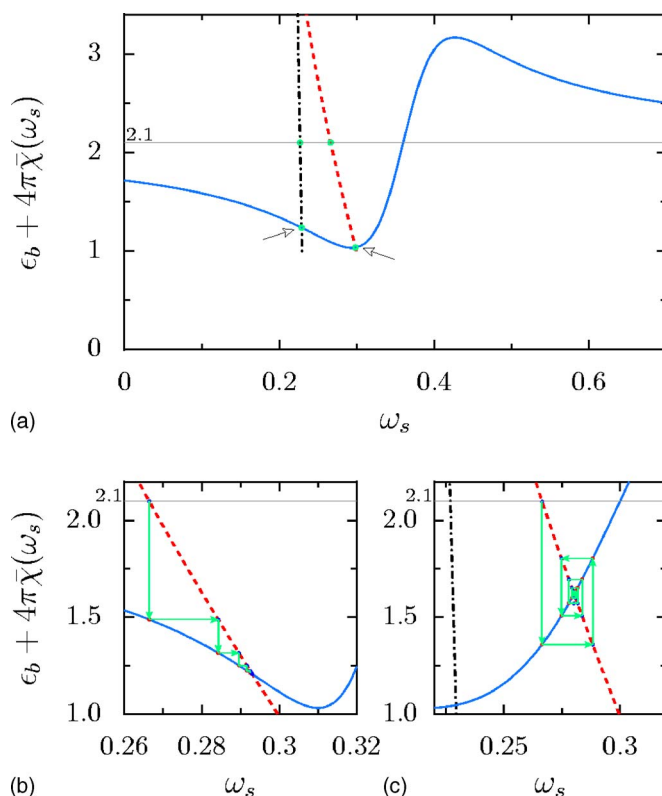


FIG. 4. (Color online) (a) Glass matrix with dielectric constant  $\epsilon_b=2.1$  is doped with atoms contributing a real, frequency-dependent susceptibility  $\bar{\chi}(\omega_s)$  given by Eq. (17a) with  $g_0=0.17$ ,  $\omega_{0s}=0.36$ ,  $\tau=15$  (solid blue line). The dielectric constant of the doped regions is positive over all frequencies and its maximum value is within the range where a number of 156 coupled Bloch modes of the BPC gave an excellent result as demonstrated in Sec. III A. Two additional lines represent the frequencies of the first band for the  $M$  point (dash-dotted black line) and the second band for the  $X$  point (dashed red line), respectively, as functions of the dielectric constant of the glass regions. The intersection of the frequency-dependent dielectric function curve with the bands (pointed to by arrows) determines the frequencies of the new bands at the  $M$  point and the  $X$  point. (b) and (c) show the convergence of an iterative method for two particular cases of the positioning of the center frequency,  $\omega_{0s}$ , and different linewidths  $\tau$  of the frequency-dependent susceptibility of the dopant atoms with regard to the band structure of the BPC. Clearly, the convergence trajectory depends sensitively on the slope of the susceptibility (solid blue line) relative to the slope of the band (dashed red line).

solving the photonic band structure in a general periodic structure where the dielectric function is frequency dependent and linear. In the CSM, the band structure for a  $d$ -dimensional periodic system is calculated in  $d+1$  dimensions, consisting of the  $d$ -dimensional Bloch wave-vector space and an extra dimension labeled as  $\epsilon$ . Here  $\epsilon$  is a hypothetical frequency-independent dielectric constant for some (or all) of the PC. The physical band structure is obtained from the intersection of the “photonic band surfaces” in  $d+1$  dimensions with a “cutting surface”  $\epsilon = \epsilon(\omega_s)$ , where  $\epsilon(\omega_s)$  is the actual frequency-dependent dielectric function. The CSM requires evaluation of photonic band structure over a large continuum of choices of  $\epsilon$ . In contrast, our it-

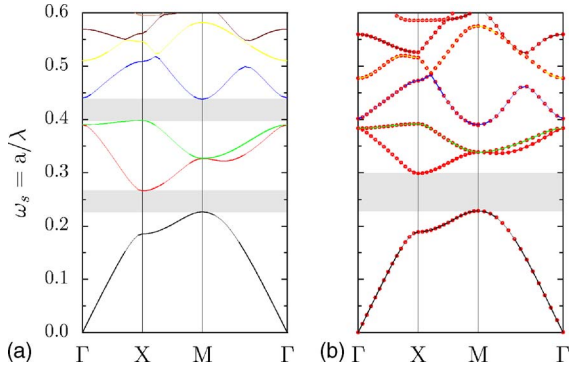


FIG. 5. (Color online) Comparison of the results obtained with our self-consistent, iterative method and these obtained by the CSM are shown on the graph (b). Graph (a) represents the photonic band structure of the BPC. The enhancement of the fundamental band gap is apparent.

erative process reduces the number of extraneous eigenvalue solutions per  $(\vec{q}, n)$  points to the number of iterations required for convergence. This is a considerable saving in computational effort for a single band structure calculation for a specific choice of the frequency-dependent dielectric. CSM, on the other hand, is well suited to calculating a large set of different band structures for different choices of the frequency dependence of the dielectric function for a fixed PC geometry. The parameters used in Eq. (17a) are  $g_0 = 0.17$ ,  $\omega_{0s} = 0.36$ ,  $\tau = 15$ . A positive value of  $g_0$  indicates inverted dopant atoms.

The agreement between the CSM and our iterative method, for the case of linear frequency-dependent dielectrics, is excellent as can be seen from Fig. 5(b). We show the number of iterations needed to reach convergence, for the seven lowest bands at the X point of the Brillouin zone, in Table II. The number of iterations shown in Table II for each  $(\vec{q}, n)$  must be compared in the CSM to the number of points in the hypothetical extra dimension of  $\epsilon$ . This is typically 30 points or more. In contrast, our iterative method typically samples only a small fraction of the points considered by CSM before converging to the final result. Most importantly, our self-consistent iterative method, unlike the CSM, is directly applicable to nonlinear and complex, frequency-dependent dielectrics as shown in the remainder of this paper.

## V. ACTIVE AND PUMPED PHOTONIC CRYSTALS: NONLINEAR EIGENMODES

### A. Nonlinear dielectric

In general the susceptibility of the dopant atoms is not only frequency dependent, it is also complex and nonlinear

TABLE II. Number of iterations needed to reach convergence for the values of eigenfrequencies, for different bands corresponding to the X point of the Brillouin first zone.

Band	1	2	3	4	5	6	7
Iterations	3	4	4	5	6	5	4

(field dependent). Moreover, in periodic microstructures used for laser light generation, the imaginary part of the dielectric function may be either positive or negative for different regions of the crystal and change sign depending on the pumping conditions. We now consider “doping” the PC with a collection of identical, homogeneously broadened three-level atomic systems. Each atom is pumped from the ground state to the third level and the third level is assumed to decay very fast (by some nonradiative relaxation process) to the second level. Under this assumption the atomic system effectively behaves as a two-level system with an imposed upper level population ([47], p. 301). If the first level of the atomic system is pumped toward the third level with a pumping rate  $R$ , it can be shown that [47,52] the susceptibility of the ensemble of dopant atoms is

$$\bar{\chi}_{dop}(\vec{r}, \omega_s) = g_0 \frac{(\omega_s - \omega_{0s})\tau_2 - i}{1 + (\omega_s - \omega_{0s})^2\tau_2^2 + \left(\frac{\Omega a}{2\pi c}\right)^2 \frac{\tau_1\tau_2}{\rho + 1}} \theta_a(\vec{r}), \quad (18a)$$

where

$$g_0 = \frac{d^2 T_2 (\rho - 1)}{\epsilon_0 \hbar (\rho + 1)} N_T. \quad (18b)$$

Here, the step function  $\theta_a(\vec{r})$  is defined in Eq. (17b),  $\rho \equiv RT_1$  is the incoherent pump parameter,  $T_1^{-1}$  is the population decay rate (by either radiative or nonradiative processes) of the second level to the ground state, and  $T_2^{-1}$  is the dephasing rate of the atomic dipole connecting the ground state and the second level. Also  $\omega_{0s} \equiv \omega_0 a / 2\pi c$ ,  $\omega_s \equiv \omega a / 2\pi c$ , and  $\tau_i \equiv 2\pi c T_i / a$  ( $i=1, 2$ ) are scaled frequencies and times,  $d$  is the electric dipole moment of the transition between the ground state and second level of the dopant atoms, and  $N_T$  is the volumetric concentration of dopant atoms.

$$\Omega \equiv \Omega_{\omega_s}(\vec{r}) \equiv \frac{dE_{\omega_s}(\vec{r})}{\hbar} \quad (18c)$$

is the position dependent Rabi frequency determined by the coupling of the atomic dipole to a self-consistently determined (Bloch mode) coherent electric field  $E_{\omega_s}(\vec{r})$  of the PC. In this situation, the output frequency [resulting from the solution of the eigenvalue problem Eq. (15)] may be complex. This corresponds to either an exponentially decaying or growing field amplitude with time.

In very high quality photonic band gap materials, the exponential population decay rate,  $1/T_1$ , may require reconsideration. For example, near a 3D band edge or other sharp jumps in local DOS, nonlocal, non-Markovian memory effects may arise [41,53,54]. A fully self-consistent treatment in a 3D PBG material would require a more detailed description of non-Markovian atomic dynamics.

The imaginary part of the susceptibility for very weak fields

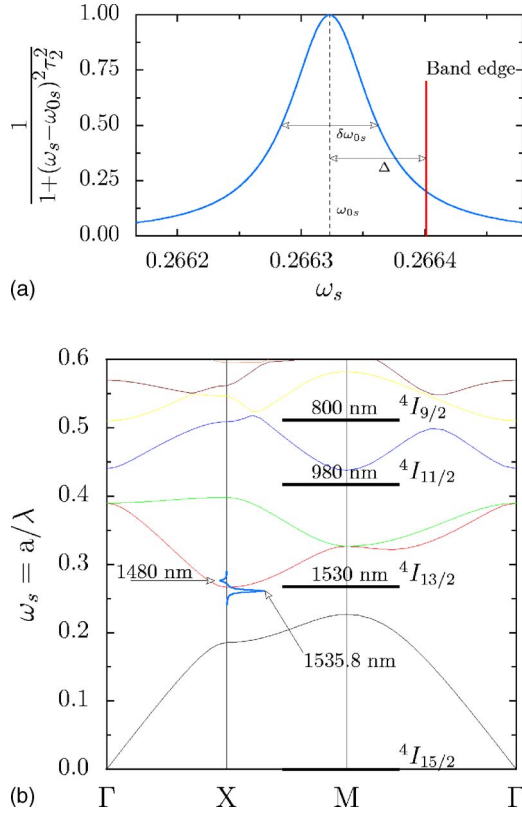


FIG. 6. (Color online) (a) Schematic graph of the imaginary part of the susceptibility of the pumped erbium ions. The frequency of the band edge [drawn in (b)] is detuned by  $\Delta = \delta\omega_{0s}$ , where  $\delta\omega_{0s}$  is the FWHM of the resonance curve, from the resonance frequency  $\omega_{0s} = 0.266323$  ( $\lambda_0 = 1535$  nm) of the  $\text{Er}^{3+}$  ions. (b) The response of the pumped erbium ions is drawn on top of the photonic band structure of the square lattice of silicon cylindrical rods ( $r = 0.3a$ ,  $\epsilon_r = 12.1$ ) in glass matrix ( $\epsilon_g = 2.1$ ). The ions absorb the pump power resonantly at  $\omega_{ps} = 0.276364$  ( $\lambda_p = 1480$  nm). The frequency of  ${}^4I_{13/2} \rightarrow {}^4I_{15/2}$  transition is situated slightly ( $\Delta = \delta\omega_{0s}$ ) within the first band gap by choosing  $a = 409$  nm. The frequency of  ${}^4I_{11/2} \rightarrow {}^4I_{15/2}$  transition is well within the second band gap, and may be an effective factor in suppressing the excitation lost by upconversion for the excited dopant atoms at high field amplitudes.

$$\bar{\chi}_{dop}''(\vec{r}, \omega_s) \approx \frac{-g_0}{1 + (\omega_s - \omega_{0s})^2 \tau_2^2} \quad (19)$$

has a full width at half maximum (FWHM)  $\delta\omega_{0s} = 2/\tau_2$ . For simplicity, we assume that all dopant atoms have the same resonance frequency  $\omega_{0s}$  (no inhomogeneous broadening). For illustration we choose the frequency  $\omega_{0s}$  within the fundamental PBG of the backbone photonic crystal and one FWHM from the upper band edge as shown in Fig. 6 top.

To provide a more realistic description, we include some small background loss in the undoped part of the BPC [Fig. 1(a), Si rods], over and above the absorption arising from the dopant atoms. This is described by a frequency-independent, position-dependent, background susceptibility within the dielectric rods

$$\bar{\chi}_{loss}(\vec{r}) = i \frac{10^{-6}}{4\pi} [1 - \theta_a(\vec{r})]. \quad (20)$$

$\bar{\chi}_{loss}$  can represent a variety of different loss mechanisms including (i) absorption loss within BPC, (ii) scattering loss into extraneous electromagnetic modes in the PC arising from small random disorder, (iii) escape into the third dimension in the case of a 2D PC of finite thickness, and (iv) radiation loss from other boundaries of a finite size PC. The total, complex, frequency- and position-dependent, nonlinear susceptibility is then given by

$$\bar{\chi}(\vec{r}, \omega_s) = \bar{\chi}_{dop}(\vec{r}, \omega_s) + \bar{\chi}_{loss}(\vec{r}). \quad (21)$$

Background susceptibility may be converted to the extinction coefficient  $\kappa$  (defined as the spatial decay rate of the magnitude of the field  $E = E_0 e^{-\kappa x} \cos[n(\omega/c)x - \omega t]$ ). In the limit of weak absorption loss ( $4\pi\bar{\chi}_{loss} \ll \epsilon$ ) the extinction coefficient becomes

$$\kappa \sim \frac{\pi \omega_s 4\pi \bar{\chi}_{loss}}{a n}.$$

Here  $\epsilon = n^2$  is the effective real dielectric constant of the photonic crystal at the scaled frequency  $\omega_s$ . Under very weak incoherent pumping, any initially excited, low amplitude, electromagnetic field will decay exponentially with time. This appears formally in our self-consistent, iterative procedure (described in Sec. IV B) by setting the Rabi field [Eq. (18c)] equal to zero in Eq. (18a). In this linear regime, the real part  $\text{Re}(\omega_s)$  of the complex output eigenfrequency is used to update the frequency,  $\omega_s$ , that appears in the self-consistent susceptibility Eq. (21).  $\text{Im}(\omega_s)$  nevertheless remains negative after the convergence of  $\text{Re}(\omega_s)$  is reached. As a result, the Bloch-mode solution for very weak pumping is a transient solution that decays exponentially to zero. In order to obtain a nontrivial solution with a purely real output eigenfrequency, it is necessary to increase the pump parameter  $\rho$  and obtain a self-consistent field amplitude  $\Omega_{\omega_s}(\vec{r})$ . This self-consistent iterative determination of *both* the field amplitude *and* the (real) eigenfrequency  $\omega_s$  is described below.

If the incoherent pumping  $\rho$  exceeds a certain threshold, the overall susceptibility given by Eq. (21) amplifies the wave rather than absorbing it. Formally this appears as an output eigenfrequency with a converged real part and a positive imaginary part. Since amplification is provided by excited atoms, growing modes for the least pumping  $\rho$  are those closest to the atomic resonance frequency  $\omega_{0s}$ . This growth can be offset by increasing  $\Omega_{\omega_s}(\vec{r})$  until it leads to a self-consistent eigenmode with a purely real output eigenfrequency. As it turns out, nonlinear eigenmodes (real self-consistent output frequency) can be generated (with sufficient pumping) for any choice of  $\omega_{0s}$ .

For illustration, we consider in detail the situation when the resonance frequency of the dopant atoms occurs at a photonic band edge. The condition that the imaginary part of the output eigenfrequency equals zero requires that we iteratively modify the field amplitude Eq. (18c). When the eigenfrequency converges to a real self-consistent steady state solution, the corresponding mode amplitude exhibits a thresholdlike behavior as a function of incoherent pumping, reminiscent of a laser input-output relation. The field  $E_q(\vec{r}, t)$

of a given Bloch vector  $\vec{q}$  (band index suppressed) may be regarded as quasimonochromatic with frequency  $\omega \equiv \omega_{\vec{q}} \equiv \omega_R + i\omega_I$  (with  $\omega_I \ll \omega_R$ ). The coefficients  $f_{\vec{q},l}$  comprising this mode [Eq. (5)] are determined by solving Eq. (15) self-consistently as described in Sec. IV B. At each intermediate stage of the iterative process (prior to self-consistency), we may write

$$E_{\vec{q}}(\vec{r}, t) = \frac{1}{2} \{ A \psi_{\vec{q}}(\vec{r}) e^{-i(\omega_R + i\omega_I)t} + A^* \psi_{\vec{q}}^*(\vec{r}) e^{i(\omega_R - i\omega_I)t} \}, \quad (22)$$

where

$$\psi_{\vec{q}}(\vec{r}) = \sum_l f_{\vec{q},l} \psi_{\vec{q},l}(\vec{r}), \quad (23)$$

$\psi_{\vec{q},l}(\vec{r})$  are eigenfunctions of the BPC, and  $A$  is the amplitude to be iteratively determined.

The field  $E_{\vec{q}}(\vec{r}, t)$  in Eq. (22) can be written as  $E_{\vec{q}}(\vec{r}, t) \equiv E_{\omega_R}(\vec{r}, t) \cos(\omega_R t - \phi)$ , where

$$E_{\omega_R}(\vec{r}, t) \equiv |A| e^{i\omega_I t} |\psi_{\vec{q}}(\vec{r})| \quad (24)$$

increases or decreases very slowly with time (quasimonochromaticity). By identifying  $\omega_R a / 2\pi c \equiv \omega_s$  and comparing to the classical expression for the electric field used in deriving Eq. (18a),  $E_{\omega_R}(\vec{r}, t)$  is the amplitude leading to the Rabi frequency Eq. (18c). In Eq. (24), both  $A$  and  $\psi_{\vec{q}}(\vec{r})$  may change from one iteration to the next.

For physical interpretation purposes, it is useful to relate this amplitude to “the number of photons,  $n_{ph}$ , per two-dimensional unit cell  $V_0$  and per unit height  $b$ .” In the following  $n_{ph}$  is referred to as simply “the number of photons per unit cell,” where the unit cell is to be understood as  $V_0 \times b$ . By integrating the time averaged electric energy density  $U_E(\vec{r}, t)$  ( $\omega_I \ll \omega_R$ ) over the 3D unit cell we obtain

$$n_{ph} = \frac{b \int_{V_0} d^2r \overline{U_E(\vec{r}, t)}}{\hbar \omega_R}. \quad (25)$$

The detailed relationship between the cycle averaged electric field energy density and the electric field amplitude Eq. (22) for a frequency-dependent dielectric function is given in Appendix B

$$U_E(\vec{r}, t) = \frac{1}{8\pi} \left. \frac{\partial[\omega \epsilon_R(\omega)]}{\partial \omega} \right|_{\omega_R} E_{\vec{q}}^2(\vec{r}, t). \quad (26)$$

Strictly speaking, this expression for the energy density is valid provided that the variation of the dielectric constant with frequency is not too large and accordingly that the imaginary part of the dielectric constant is relatively small. If this is not satisfied, the more general expression Eq. (B5) must be considered. For convenience, we normalize the nonlinear Bloch modes according to the relation

$$\frac{1}{V_0} \int_{V_0} d^2r \psi_{\vec{q}}^*(\vec{r}) \left. \frac{\partial[\omega \epsilon_R(\omega)]}{\partial \omega} \right|_{\omega_R} \psi_{\vec{q}}(\vec{r}) \equiv 1, \quad (27)$$

where  $V_0$  is the volume of the unit cell. Inserting Eq. (22) into Eq. (26) and that into Eq. (25) after performing the time average, we obtain

$$V_0 b \frac{|A|^2 e^{2\omega_I t}}{16\pi} = \hbar \omega_R n_{ph}. \quad (28)$$

Here, we have used the periodicity of  $\psi_{\vec{q}}(\vec{r})$  and  $\epsilon_R$ . In case of frequency-independent dielectric function, Eq. (27) reduces to the conventional normalization equation [Appendix A, Eq. (A2)]. Using Eqs. (27), (28), and (24) we obtain (after converting to SI units)

$$E_{\omega_R}^2(\vec{r}, t) \equiv |A|^2 e^{2\omega_I t} |\psi_{\vec{q}}(\vec{r})|^2 = \frac{4}{\epsilon_0 V_0 b} \hbar \omega_R n_{ph} |\psi_{\vec{q}}(\vec{r})|^2 \quad (29)$$

with the understanding that the number of photons per unit cell  $n_{ph}$  of frequency  $\omega_R$  increases if  $\omega_I > 0$  and decreases if  $\omega_I < 0$ , and  $\psi_{\vec{q}}(\vec{r})$  is normalized according to Eq. (27). In what follows we refer to the number of photons per unit cell,  $n_{ph}$ , rather than the electric field amplitude in our iterative self-consistent field method to obtain a real output eigenfrequency.

We introduce the position and frequency-dependent mode intensity

$$I_{\omega_s}(\vec{r}) \equiv n_{ph} \frac{2d^2 \omega_{0s}}{\pi \hbar c \epsilon_0 a b (\rho + 1)} |\psi_{\vec{q}}(\vec{r})|^2, \quad (30)$$

where  $\omega_s \equiv \omega_R a / 2\pi c$ , and rewrite Eq. (18a) as

$$\bar{\chi}_{dop}(\vec{r}, \omega_s) = g_0 \frac{(\omega_s - \omega_{0s}) \tau_2 - i}{1 + (\omega_s - \omega_{0s})^2 \tau_2^2 + I_{\omega_s}(\vec{r}) \omega_s \omega_{0s}^{-1}} \theta_a(\vec{r}). \quad (31)$$

Population inversion of the dopant atoms is likewise position dependent and is given by [47,52]

$$w(\vec{r}) = \frac{1 + (\omega_s - \omega_{0s})^2 \tau_2^2}{1 + (\omega_s - \omega_{0s})^2 \tau_2^2 + I_{\omega_s}(\vec{r}) \omega_s \omega_{0s}^{-1}} \frac{(\rho - 1)}{(\rho + 1)}. \quad (32)$$

The averaged population inversion is given by the formula  $\bar{w} = 1/V_{0d} \int_{V_{0d}} d^2r w(\vec{r})$  where  $V_{0d}$  represents the part of the volume of the unit cell doped with active atoms.

## B. Self-consistent method

We now outline the complete iterative process to obtain an exact self-consistent Bloch-mode solution to the nonlinear wave equation [Eq. (15)] in the strongly scattering photonic crystal doped with two-level atoms and with some background loss. This consists of three stages.

(1) As in the linear wave equation problems of Secs. III and IV, we begin by calculating the band structure of BPC with the “dopants switched off” [ $\bar{\chi}_{dop}(\vec{r}, \omega_s) \equiv 0$ ] and no background loss [ $\bar{\chi}_{loss}(\vec{r}) \equiv 0$ ]. Here the BPC is defined as that part of the entire dielectric profile which is linear and frequency independent. It may include the region where the resonant doping constituents will later be introduced. For each Bloch vector and band,  $(\vec{q}, n)$ , we calculate the eigenfrequency and the field distribution using our integral equation formalism. They are the same as if found with PWE calculations. The BPC Bloch modes are normalized according to Eq. (27).

(2) For simplicity, we consider all dopant atoms to have the same resonance frequency,  $\omega_{0s}$ . This remains fixed throughout the calculation. In other words, homogeneous line broadening of the atomic transition is assumed to be dominant compared to inhomogeneous line broadening. The dielectric constant of the BPC is then supplemented by the contribution from the dopant atoms [Eq. (31)] and background loss [Eq. (34)]. We now choose a particular incoherent pumping level  $\rho$ , and particular  $(\vec{q}, n)$  at which we wish to obtain a self-consistent nonlinear Bloch wave. The susceptibility of the dopant atoms in iteration  $m+1$  is obtained by inserting the real part  $\text{Re}(\omega_{s,m})$  of the output frequency and the normalized Bloch mode (defined through Eqs. (23) and (27) of that particular  $(\vec{q}, n)$  position, obtained in iteration  $m$ . For the initial guess, we choose an infinitesimal number of photons per unit cell,  $n_{ph}=5 \times 10^{-6}$  and enter this choice into Eq. (30). We then solve the integral equation (15) iteratively until the real part of the output frequency  $\omega_{s,m+1}$  converges to  $\omega_{s,m}$ . We normalize the output Bloch mode Eq. (23) in accordance with Eq. (27) in every iteration step. The condition for the convergence in step 2 is that  $|\text{Re}(\omega_{s,m+1}) - \text{Re}(\omega_{s,m})| < 10^{-14}$ . However, the solution obtained in stage 2 is not necessarily an eigenmode of the system (which by definition is a steady state solution with purely real eigenfrequency). To obtain a true eigenmode it is necessary to converge to a self-consistent field amplitude in which the imaginary part of the output frequency is also zero.

(3) After the convergence of the real part of the mode frequency is achieved in stage 2, the imaginary part of the output frequency may be nonzero due to absorption and emission of light from the dopant atoms and the background loss. Such a solution is not a self-consistent, steady state solution of Maxwell's equations. In general, this is only a transient state that decays to zero or evolves into a different type of mode. If  $\text{Im}(\omega_{s,m+1}) < 0$ , the output mode decays exponentially to zero. This suggests that for the chosen incoherent pumping level  $\rho$ , the only self-consistent, steady state solution is zero. In order to find a nontrivial solution, we then increase the pumping level incrementally and repeat the procedure described in stage 2. For sufficiently strong incoherent pumping, the output frequency of stage 2 [with converged  $\text{Re}(\omega_{s,m+1})$ ] exhibits a positive imaginary part [ $\text{Im}(\omega_{s,m+1}) > 0$ ]. In this case, a steady state nonlinear eigenmode may be found by increasing the number of photons per unit cell,  $n_{ph}$ , appearing in Eq. (30). After increasing the number of photons per unit cell, we repeat the iterative procedure (described in stage 2) now with a new convergence criterion: both  $|\text{Re}(\omega_{s,m+1}) - \text{Re}(\omega_{s,m})| < 10^{-14}$  and  $|\text{Im}(\omega_{s,m+1})| < 10^{-14}$  must be satisfied for the iteration to stop. In practice about 50 iterations are required in steps 2 and 3.

Convergence reached in stage 3 yields a final, self-consistent number of photons per unit cell,  $n_{ph}$ , required to produce a self-consistent Bloch wave with purely real frequency. We refer to this steady state Bloch wave in the complex, nonlinear dielectric medium as a nonlinear eigenmode.

In practice, a modified iterative procedure (described below) is useful to treat strong nonlinearities and high dopant concentrations. The modification consists in changing the initial conditions in stage 2. In particular, the iteration is

initialized using a photon number per unit cell and field configuration obtained from the converged nonlinear Bloch wave of a smaller incoherent pumping level. This modified iterative procedure overcomes convergence problems in stage 2 that occur for strong coupling situations involving colloidal quantum dots (see Sec. VI C).

## VI. APPLICATION OF THE NONLINEAR EIGENMODES METHOD

In this section, we consider three specific models of resonantly doped photonic crystals corresponding to successively larger perturbations of the backbone PC and varying degrees of background loss. In each case, we demonstrate the occurrence of self-consistent nonlinear Bloch waves with purely real eigenfrequency for sufficient pumping.

### A. Erbium doped silica-silicon PC

Consider doping the PC with triply ionized erbium atoms  $\text{Er}^{3+}$  with a volumetric concentration  $N_T \cong 1.0 \times 10^{19} \text{ cm}^{-3}$  in a glass matrix surrounding silicon rods as shown in Fig. 1(a). In order to position the resonance frequency of  $\lambda_0 = 1535.8 \text{ nm}$  of the erbium atoms within the first band gap and one FWHM away from the band edge of the second band at the  $X$  point (Fig. 6 top), we choose a photonic crystal lattice constant  $a=409 \text{ nm}$  (Appendix C). The unit height in the direction out of plane of the periodicity is taken as  $b=a$ .

Results of our self-consistent method are presented in Fig. 7. For a background loss  $4\pi\bar{\chi}_{loss} = i10^{-6}$ , there is a threshold incoherent pumping level ( $\rho_{th} \cong 1.053$ ), beyond which self-consistent, nonlinear Bloch waves appear in the second band at  $\vec{q}=X$  point. The threshold pumping  $\rho_{th}$  increases with the detuning of the BPC eigenmode frequency from the resonance frequency of the dopant atoms while the resonant frequency remains inside the band gap as shown in Fig. 8. As expected, the threshold,  $\rho_{th}$ , increases as the background loss  $\bar{\chi}_{loss}$  increases (Fig. 12), and decreases as the volumetric concentration  $N_T$  of the dopant atoms increases. We observe that beyond a background loss of  $4\pi\bar{\chi}_{loss} \cong i4.5 \times 10^{-5}$ , for fixed  $N_T=1.0 \times 10^{19} \text{ cm}^{-3}$  and quantum dot detuning from the  $X$ -point band edge, there are no self-consistent solutions transition threshold ( $\rho_{th} \rightarrow \infty$ ). In other words, when the background loss is too large, there are no nonlinear Bloch waves in the system. This occurs when loss is only roughly 12% of gain ( $\text{loss/gain} \sim [\text{Im}(\bar{\chi}_{loss})A_{loss}]/[\text{Im}(\bar{\chi}_{dop})A_{dop}] \sim 0.12$  for  $A_{loss} = \pi r^2 = \pi(0.3a)^2$ ,  $A_{dop} = a^2 - A_{loss}$ ,  $g_0 \cong 5.92 \times 10^{-5}$ , and one FWHM detuning).

For  $4\pi\bar{\chi}_{loss} \cong i10^{-5}$  and below the threshold  $\rho_{th} \cong 1.053$ , the solutions to Maxwell's equation with Bloch vector  $\vec{q}=X$  point are transients that decay to zero with time [Fig. 7(d)]. Above the threshold, a nonlinear Bloch wave with real frequency emerges that clamps to a value  $\omega_s \cong 0.2664007$  despite further increases in the pumping power. As shown in Fig. 7(c), the self-consistent nonlinear eigenmode frequency is shifted by about 0.2 GHz from the band edge at  $\omega_s \cong 0.266401$  of the undoped BPC. The number of photons per unit cell increases almost linearly with the pump parameter above the threshold as shown in Fig. 7(a).

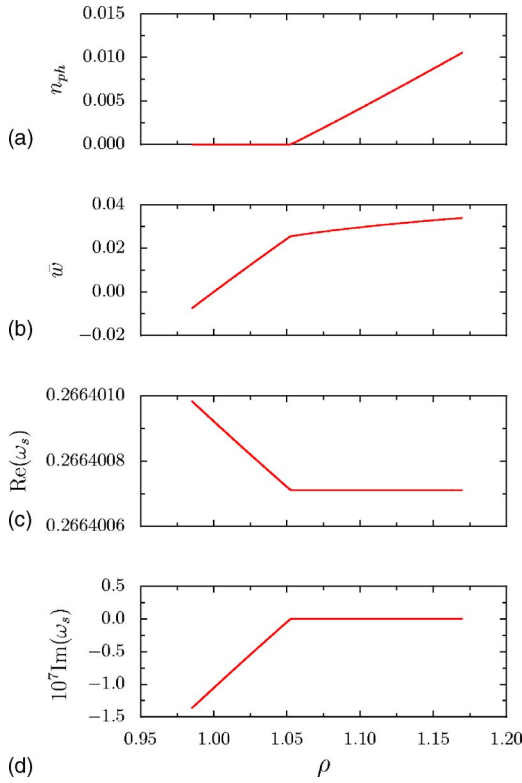


FIG. 7. (Color online) Photonic crystal of Fig. 1(a), with lossy silicon rods ( $4\pi\bar{\chi}_{loss}=i10^{-6}$ ) and dopant erbium ions under pumping  $\rho$ . Shown are (a) the number of photons per unit cell,  $n_{ph}$ , corresponding to the self-consistent field of the second band at the X point, (b) average inversion  $\bar{w}$  of the dopant atoms, (c) the real part of the frequency of the second band at the X point, and (d) the imaginary part of the frequency of the second band at the X point—as functions of the pumping parameter  $\rho$ .

In Fig. 9 we show the expansion coefficients, by which the self-consistent nonlinear Bloch wave at the X point of the second band is represented in the basis of eigenmodes of the BPC (silicon-silica undoped photonic crystal). Most coeffi-

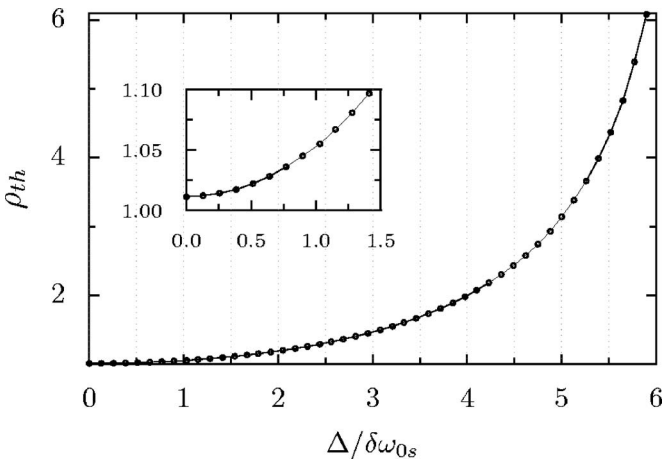


FIG. 8. Threshold pump  $\rho_{th}$  increases as the resonance frequency of the erbium ions is moved deeper into the band gap. The detuning  $\Delta$  of the resonance frequency of the erbium ions from the band edge is measured in terms of the FWHM,  $\delta\omega_{0s}$ , of that resonance.

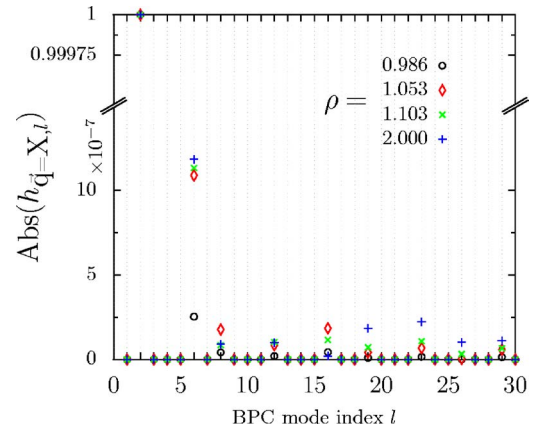


FIG. 9. (Color online) Coupling coefficients  $\{h_{\vec{q}_i}\}$  for  $\vec{q}$  at the X point and the second photonic band of the doped BPC as the pump parameter is increased and the convergence is reached.

icients are very small as expected because the overall perturbation is very weak. For illustration we plot in Fig. 10 the absolute value of the electric field for some of the eigenmodes of the BPC that are coupled to the active atoms. The evolution of the self-consistent nonlinear Bloch wave, as the pumping  $\rho$  is increased, is shown in Fig. 11. Since the perturbation is very weak, the nonlinear Bloch wave resembles the BPC eigenmode. We draw the absolute value of the difference of the electric field between the nonlinear Bloch wave and the BPC eigenmode at the X point (second band) for various pumps  $\rho$ .

In Fig. 12 we show how the number of photons per unit cell,  $n_{ph}$ , varies with the pump parameter, for different losses in silicon rods while the resonance frequency of the two-level atoms is kept fixed at one FWHM away from the X-point band edge.

In Fig. 13 we show how the number of photons per unit cell,  $n_{ph}$ , varies as the resonance frequency of the two-level atoms is positioned at different scaled frequencies. We observe that the transition threshold is the smallest for the

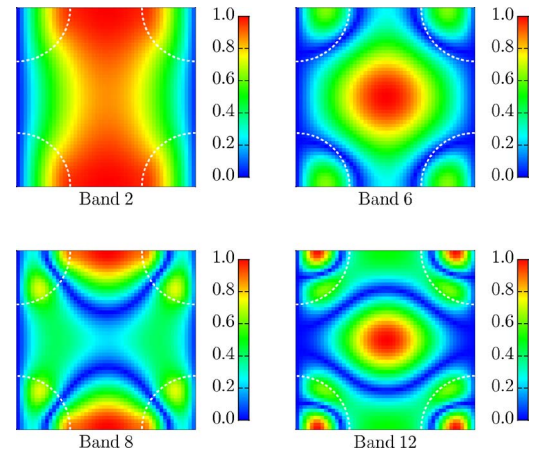


FIG. 10. (Color online) The absolute value of the electric field of Bloch modes corresponding to bands 2, 6, 8, 12, and with the Bloch vector ending at the X point of the Brillouin zone are drawn. The white dashed lines show the dielectric boundaries.

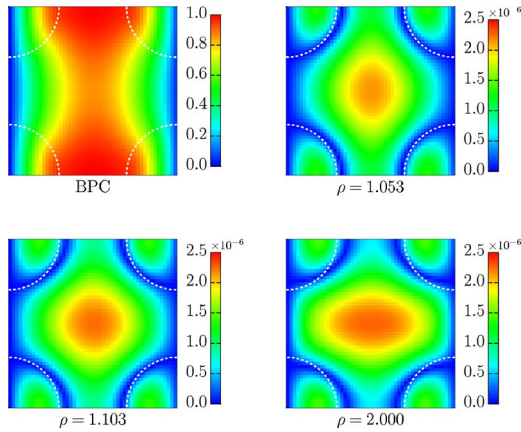


FIG. 11. (Color online) If the normalized nonlinear Bloch field obtained at the end of the convergence procedure, step 3 (as described in Sec. V) is drawn for different values of the pump parameter ( $\rho=1.053$ —at the threshold, 1.103—above threshold, 2.000—well above threshold), a very minor change from the eigenmode of the backbone photonic crystal can be observed. Nevertheless the absolute value of the difference of the normalized fields with the BPC eigenmode, for different pumps, reveals the differences. The absolute value of the difference of the normalized nonlinear Bloch field with the BPC eigenmode (upper left picture) for  $\rho=1.053$  (upper right picture),  $\rho=1.103$  (lower left picture), and  $\rho=2.000$  (lower right picture) has a small magnitude of the order of  $2 \times 10^{-5}$ . The white dashed lines show the dielectric boundaries.

X-point band edge. The rate of increase (average slope) of the number of photons per unit cell with pumping is very sensitive to the positioning of the resonance frequency as shown in the inset of Fig. 13(b). In calculating the average slope we have gone up to a pump  $\rho=32.1$ .

In Fig. 14 the converged self-consistent field modifications at the four  $\vec{q}$ -points labeled in Fig. 13(b) are drawn for a pump value of  $\rho=12.1$ . The nonlinear modification of the BPC field for the second band and Bloch vectors  $\vec{q}=2, 15(X \text{ point})$ , and 44 is small in comparison with the order of unity modification of the BPC field at  $\vec{q}=30(M \text{ point})$ . Due to the degeneracy of the modes at  $\vec{q}=30$ , it is possible for the dopant atoms to scatter light between the degenerate modes (bands 2 and 3) at the  $M$  point, resulting in a large overall change in the field pattern.

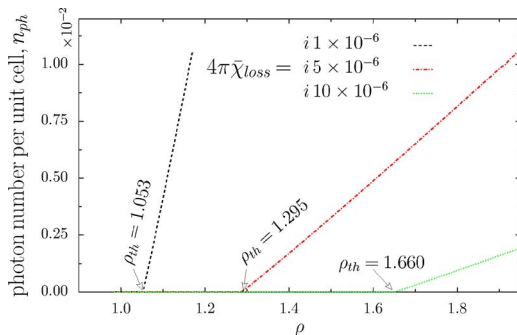


FIG. 12. (Color online) Dependence of the threshold for the pump parameter and the slope of the number of photons per unit cell versus the pump parameter, when the losses are varied.

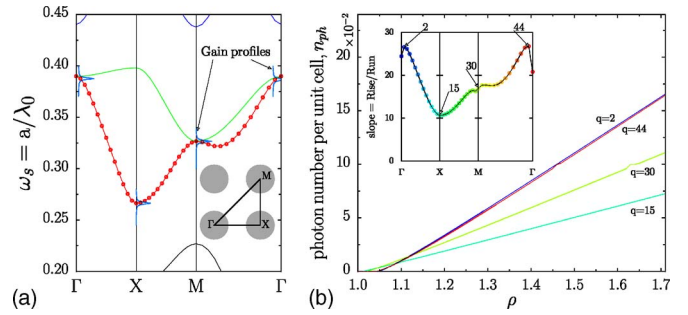


FIG. 13. (Color online) (a) The resonance frequency of the homogeneously broadened transition of two level atoms is positioned at different frequencies of the second band of the backbone photonic crystal. (b) Transition threshold for the pump parameter and the slope of the dependency of the number of photons per unit cell versus the pump parameter differs for different positioning of the resonance frequency with regard to the second band. Average slopes are calculated at 45 points (15 Bloch vectors per each direction) around the boundaries of the first Brillouin zone. For clarity, only four slopes, corresponding to the resonance frequency positioned close to  $\Gamma$  points ( $\vec{q}=2, 44$ ) and exactly at the  $X$  and  $M$  band edges ( $\vec{q}=15, 30$ ), are drawn. The inset shows how the slopes of the photon number per unit cell versus pumping vary as the resonance frequency is positioned on the boundary of the first Brillouin zone. The singularity and therefore the numerical accuracy of the calculations at the  $\Gamma$  point may explain why the slopes there show discontinuities.

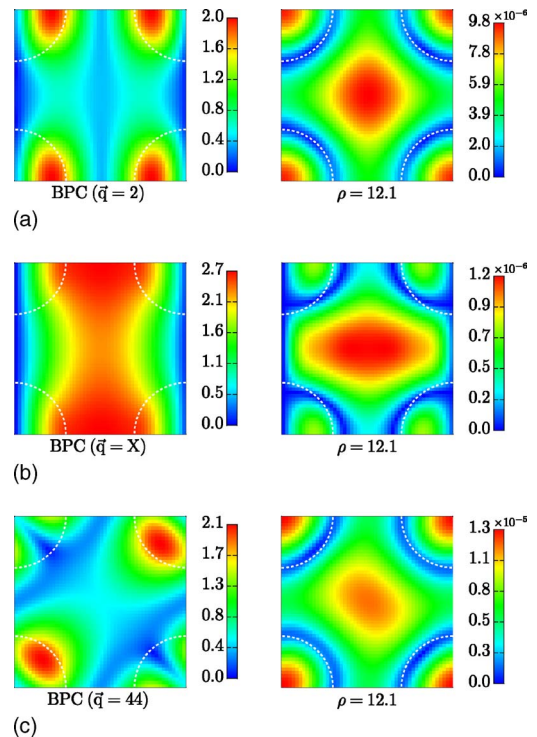


FIG. 14. (Color online) This picture complements the inset of Fig. 13(b). Backbone photonic crystal fields for the second photonic band and Bloch vectors 2, 15, and 44 are drawn in the first column. The respective absolute values of the difference of the electric vector of the converged fields under pump  $\rho=12.1$  with the electric vector of the BPC is drawn in the second column.

As described in standard textbooks ([47], p. 307) the minimum optical pumping power density necessary to establish the threshold inversion is given by

$$(Pwr/V)_{th} = (V_{0d}/V_0)\hbar\omega_p(N_1)_{th}R_{th},$$

where  $(N_1)_{th}$  is the number of the dopant atoms in ground level at threshold pumping,  $R_{th}$  is the rate of pumping at threshold,  $V_{0d}/V_0$  is the volume fraction of the active region of the PC unit cell, and  $\omega_p$  is the optical pumping frequency to the third atomic level, from which there is a rapid decay to the second level situated at  $\omega_{0s}$ . Using  $N_1 = N_T/(1 + RT_1)$  where  $N_T$  is the volumetric concentration of the resonant two-level systems (valid for negligible values of stimulated emission) we obtain a threshold optical pump power density of roughly  $6.7 \times 10^{-11} \text{ W}/\mu\text{m}^3$  for the emergence of nonlinear Bloch waves in this “weak coupling” system of erbium light emitters. As expected, the pump power required to reach the threshold is inversely proportional to the population decay time  $T_1$ . For 3D PC, and the resonance frequency of the dopant atoms situated within the complete PBG but coupled to a single mode wave guide, the decay rate  $T_1^{-1}$  may be reduced drastically. In this case, the pump power required to establish a steady state nonlinear Bloch wave in an erbium doped PBG microchip wave-guide channel may be correspondingly reduced.

### B. Thin coating shell of colloidal quantum dots in silicon PC

As a second illustration, we consider a photonic crystal consisting of a square array of vertical air pores of radius  $r = 0.45a$  (where  $a$  is the side of the square unit cell) etched onto a silicon matrix. As a radiative system embedded in the BPC we consider quantum dots, coating the inner surfaces of the air pores, forming a shell of thickness  $\delta = 0.04a$ , as shown in Fig. 1(b). The dielectric constant  $\epsilon_c = 6.0$  represents the frequency-independent part of the dielectric function of the quantum dots. Quantum dots are considered to be spheres of diameter 5 nm, encapsulated with a polymeric capping group (spherical shell) of thickness 2 nm that prevents adjacent dots to touch each other. The volumetric density (calculated for a fcc close packing of encapsulated quantum dots) is  $N_T \approx 9.7 \times 10^{17} \text{ cm}^{-3}$  (see Appendix D).

Specific physical realizations of this system include PbS and PbSe colloidal quantum dots [55]. We assume that the resonance wavelength of the quantum dots is  $\lambda_0 = 1.55 \mu\text{m}$ , with homogeneous line broadening  $\delta\lambda/\lambda_0 \approx 0.17\%$ . We neglect inhomogeneous line broadening in order to simplify the illustration and the computation. The separation of 4 nm ensured by the capping groups prevents direct charge transfer between adjacent dots. The frequency-dependent part of the dielectric function of the ensemble of quantum dots is given by

$$\bar{\chi}_{coat}(\vec{r}, \omega_s) = g_0 \frac{(\omega_s - \omega_{0s})\tau_2 - i}{1 + (\omega_s - \omega_{0s})^2\tau_2^2 + I_{\omega_s}(\vec{r})\omega_s\omega_{0s}^{-1}} \theta_c(\vec{r}), \quad (33a)$$

where

$$\theta_c(\vec{r}) = \begin{cases} 1, & \text{for } \vec{r} \text{ pointing within the coating,} \\ 0 & \text{otherwise.} \end{cases} \quad (33b)$$

The other parameters of Eq. (33a) are  $\tau_2 = 5.1 \times 10^3$ ,  $g_0 = 0.44(\rho - 1)/(\rho + 1)$ ,  $I_{\omega_s}(\vec{r}) = n_{ph} 1.75 \times 10^{-2}/\omega_{0s}^3(\rho + 1)|\psi_{\vec{q}}(\vec{r})|^2$  where  $n_{ph}$  is the number of photons per unit cell and  $\rho$  is the pump parameter (see Appendix D for details of the choice of parameters). The FWHM of the gain spectrum is  $\delta\omega_{0s} = 2/\tau_2 = 0.0004$ . We situate the resonance frequency of quantum dots within the first band gap which extends from  $\omega_s = 0.22324$  (first photonic band,  $M$  point) to  $\omega_s = 0.24321$  (second photonic band,  $X$  point), one FWHM away from the  $X$ -point band edge, at a scaled frequency  $\omega_{0s} = 0.2428$  as shown in Fig. 15. This is implemented by choosing the lattice constant  $a \approx 370 \text{ nm}$  and the thickness of the quantum dot coating shell  $\sim 15 \text{ nm}$  (roughly two layers of quantum dots are coating all the inner surfaces of the silicon microstructure). In addition we include a distributed background loss, outside the colloidal quantum dot coating layers, through the background susceptibility

$$\bar{\chi}_{loss}(\vec{r}) = i \frac{10^{-4}}{4\pi} [1 - \theta_c(\vec{r})]. \quad (34)$$

In our present calculation we chose a value of  $T_1^{-1}$  corresponding to an ordinary (nearly featureless) electromagnetic density of states. We set  $T_1 = 1 \text{ ns}$  in accordance with the observed Auger recombination time scale in quantum dots [56]. The close proximity of the resonance frequency to the band edge offers the possibility of substantial gain and 2D distributed feedback. This is sufficient to overcome other losses (represented by  $\bar{\chi}_{loss}$ ) and sustain nonlinear Bloch waves with purely real frequency.

Results of our modified self-consistent iterative method are presented in Fig. 16. The threshold incoherent pumping is  $\rho_{th} \approx 1.008$ . Below the threshold, the solution to Maxwell's equation with Bloch vector  $\vec{q} = X$  point is a transient that simply decays to zero [Fig. 16(d)]. Above the threshold, a nonlinear Bloch wave with real frequency emerges and clamps to a frequency  $\omega_s \approx 0.24319$  despite further increases in the pumping power. The number of photons per unit cell increases almost linearly with the pump parameter above the threshold as shown in Fig. 16(a). A rough estimate of the average electric field intensity of the nonlinear Bloch wave is  $E \sim 2.1 \sqrt{n_{ph}} \omega_s / na^2 \times 10^3 \text{ V/cm}$ , where  $\omega_s$  is the scaled frequency of the nonlinear Bloch wave,  $n_{ph}$  is the number of photons per unit cell,  $n$  is the average refractive index of the unit cell, and  $a$  is the side of the unit cell in  $\mu\text{m}$ . In particular, we get  $E \sim 1.9 \times 10^3 \text{ V/cm}$  for  $n_{ph} \sim 1$ ,  $a = 0.37$ ,  $\omega_s \sim 0.24185$ , and  $n \sim 4$ . In our calculations, the iteration procedure of the third step is terminated after 60 iterations if the convergence criterion  $|\text{Im}(\omega_{s,m+1})| < 10^{-14}$  (see Sec. V) is not reached. In practice, we reach a level of convergence for the imaginary part of frequency of the Bloch wave of only  $|\text{Im}(\omega_{s,m+1})| < 10^{-7}$  for some pump values. As expected, the threshold  $\rho_{th}$  increases as the background loss  $\bar{\chi}_{loss}$  increases as can be seen from Fig. 17.

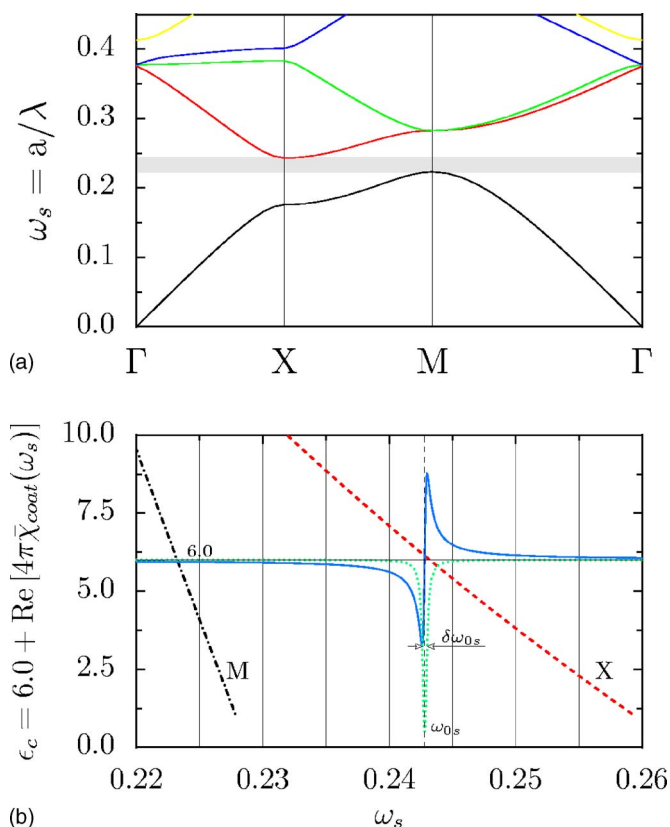


FIG. 15. (Color online) (a) The BPC photonic band structure for the case of Fig. 1(b). A band gap for the  $E$ -polarized fields extends from  $\omega_s=0.2232$  (first photonic band,  $M$  point) to  $\omega_s=0.2432$  (second photonic band,  $X$  point). (b) The coating shell of Fig. 1(b) has a susceptibility  $\bar{\chi}_{coat}(\omega_s)$  defined by Eq. (33a) with coefficients  $\omega_{0s}=0.2328$ ,  $\tau_2=5100$ ,  $g_0=0.44$  (infinite pumping). The real (solid blue line) and the imaginary (dotted green line, plotted close to the real part for clarity) part of the susceptibility of the ensemble of quantum dots are drawn for the very weak field. Two additional lines represent the frequencies of the first band for the  $M$  point (dash-dotted black line) and the second band for the  $X$  point (dashed red line), respectively, as the dielectric constant of the coating shell is varied.

### C. Thick coating shell of colloidal quantum dots in silicon PC

Finally we consider of situation where the dopants constitute a relatively large perturbation of the original BPC. We consider the same situation as in the previous subsection but now the thickness of the shell of quantum dots is  $\delta=0.12a$ , as shown in Fig. 1(c). For the BPC of Fig. 1(c) a very small band gap ( $\approx 1\%$  of the center frequency) extends from  $\omega_s=0.2186$  (first photonic band,  $M$  point) to  $\omega_s=0.2209$  (second photonic band,  $X$  point) as can be seen in Fig. 18. We situate the resonance frequency of quantum dots in the center of the band gap at the scaled frequency  $\omega_{0s}=0.2197$ . This situation is achieved using a photonic crystal with a lattice constant  $a \approx 341$  nm. The resonant part of the dielectric function of the quantum dots is given by Eqs. (33a) and (33b), with parameters  $\omega_{0s}=0.2197$ ,  $\tau_2=5100$ ,  $g_0=0.44(\rho-1)/(\rho+1)$ ,  $I_{\omega_s}(\vec{r})=n_{ph}1.76 \times 10^{-2}/\omega_{0s}^3(\rho+1)|\psi_q(\vec{r})|^2$  where  $n_{ph}$  is

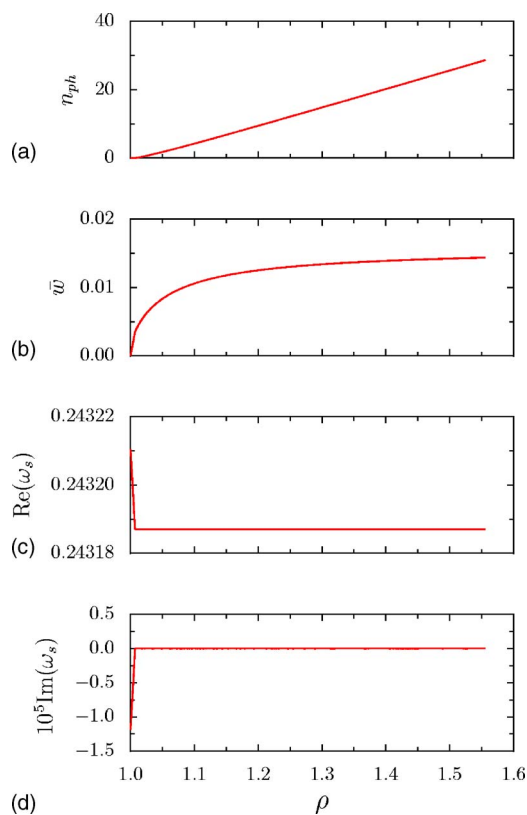


FIG. 16. (Color online) (a) The number of photons per unit cell  $n_{ph}$ , (b) average inversion  $\bar{w}$  of the dopant atoms, (c) the real part of the frequency of the second band at the  $X$  point, and (d) the imaginary part of the frequency of the second band at the  $X$  point—as functions of the pumping parameter  $\rho$ .

the number of photons per unit cell, and  $\rho$  is the pump parameter (see Appendix D). In addition we include a distributed background loss, present everywhere in the unit cell except the coating shell, through the background susceptibility

$$\bar{\chi}_{loss}(\vec{r}) = i \frac{5 \times 10^{-4}}{4\pi} [1 - \theta_c(\vec{r})]. \quad (35)$$

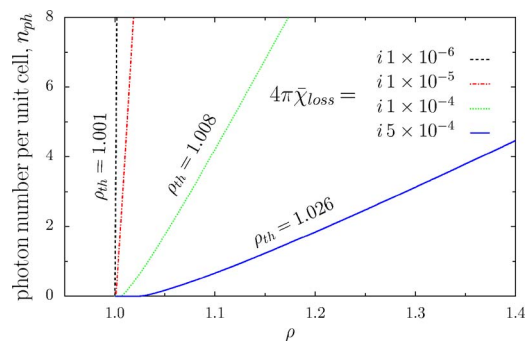


FIG. 17. (Color online) Threshold and photon density behavior as the background loss is varied. 156 lowest (in frequency) plane waves of the BPC are considered coupled from the spatial distribution of the resonant colloidal quantum dots and the background loss.

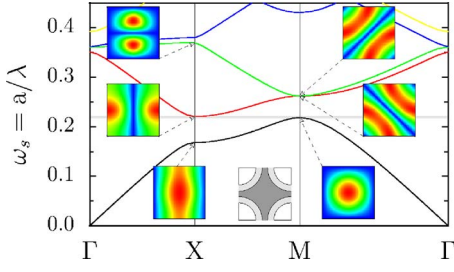


FIG. 18. (Color online) Photonic band structure of the  $E$ -polarized field in the BPC with unit cell as shown in the gray scale inset. A tiny band gap extends from  $\omega_s=0.2186$  (first photonic band,  $M$  point) to  $\omega_s=0.2209$  (second photonic band,  $X$  point). The absolute value of the electric field for the normalized Bloch eigenmodes is drawn for three first bands at points  $X$  and  $M$  of the first Brillouin zone.

In Fig. 19, the real part of the susceptibility of the ensemble of quantum dots is drawn for two values of the pump  $\rho=1.2$  and  $2.0$  and for very weak fields. The unmodified iteration procedure of stage 2 (described in Sec. V) exhibits convergence problems because the slope of the real part of the susceptibility (for very weak fields) is large compared to the slope of the band edge at the  $X$  point (dashed red line). In this situation of large imaginary parts of the resonant susceptibility, it is problematic to define a normalization for the electromagnetic field for certain frequency and pump regions. The expression  $\partial[\omega\epsilon_R(\omega)]/\partial\omega$  as defined in Eq. (B5) is negative for very weak fields, indicating a breakdown of the approximation leading from Eq. (B5) to Eqs. (B6)–(B8). For such large imaginary parts of the dielectric response, the

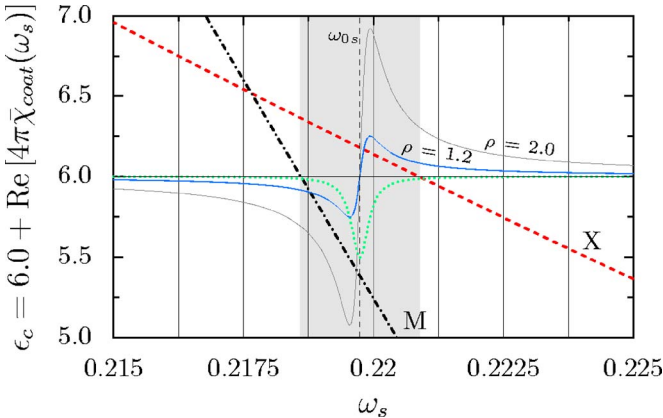


FIG. 19. (Color online) The shell formed from quantum dots coating the inner surfaces of the air pores, shown in Fig. 1(c), has a susceptibility  $\bar{\chi}_{coat}(\omega_s)$  defined by Eq. (33) with coefficients  $\omega_{0s}=0.2197$ ,  $\tau_2=5100$ ,  $g_0=0.44(\rho-1)/(\rho+1)$ . The real part (solid blue line) and the imaginary part (dotted green line, shifted close to the real part for clarity) of the susceptibility of the shell of quantum dots are drawn for pump  $\rho=1.2$  and  $n_{ph}=0$ . The real part of susceptibility is drawn (solid gray line) for another pump value,  $\rho=2.0$  and  $n_{ph}=0$ . Two additional lines represent the frequencies of the first band for the  $M$  point (dash-dotted black line) and the second band for the  $X$  point (dashed red line), respectively, for a frequency independent BPC, as the dielectric constant of the coating shell is varied.

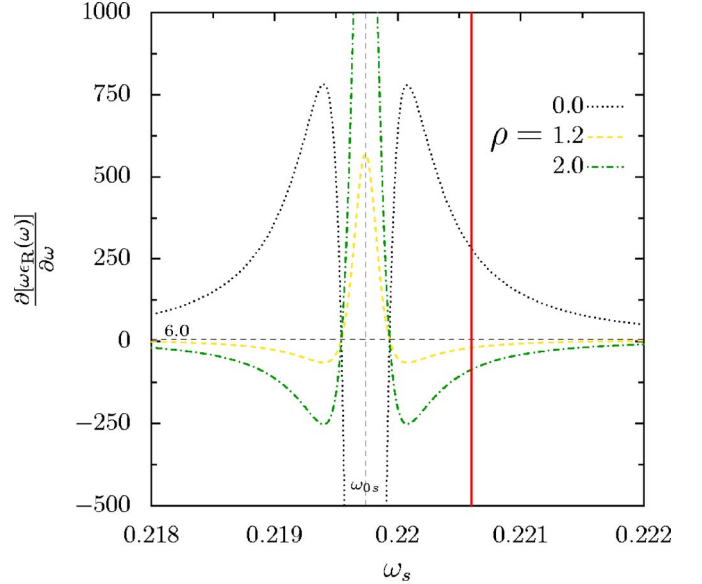


FIG. 20. (Color online) The spatial normalization of the quasi-monochromatic electromagnetic field, as defined in Eq. (28), requires a positive value for the function  $\partial[\omega\epsilon_R(\omega)]/\partial\omega$  [see Eq. (C5)]. This function is plotted above for the case of very weak fields ( $n_{ph}\approx 0$ ) and pump values  $\rho=0, 1.2$ , and  $2$ . The red vertical line represents the frequency position (roughly) of the second band at the  $X$  point. As shown in this graph, the normalization of the band edge field may not be performed for very weak fields and pumps above a certain value, due to  $\partial[\omega\epsilon_R(\omega)]/\partial\omega$  being negative. This problem is overcome using the modified iteration procedure.

field is no longer quasimonochromatic. In this case, we must either use the exact relation Eq. (B5) to obtain the electromagnetic energy density or we must use the modified iteration scheme alluded to at the end of Sec. V. We choose the latter option.

Using the modified iteration procedure, the normalization [Eq. (27)] is successful and self-consistent, nonlinear, Bloch waves are obtained. In practice, the iteration procedure of the modified stage 2 is terminated after 15 iterations if the convergence criterion  $|\text{Re}(\omega_{s,m+1})-\text{Re}(\omega_{s,m})|<10^{-14}$  is not reached and the iterative procedure of stage 3 is terminated after 60 iterations if  $|\text{Im}(\omega_{s,m+1})|<10^{-14}$  (see Sec. V) is not reached (usually the convergence criterion on  $|\text{Re}(\omega_{s,m+1})-\text{Re}(\omega_{s,m})|<10^{-14}$  in stage 3 is met). This “slow” convergence sometimes occurs for strong active medium–field interaction and strong background loss. In such cases, we relax the convergence criterion slightly.

In Fig. 21 the growth of the number of photons per unit cell,  $n_{ph}$ , as the pump is increased is slower than of the thin coating layer represented in the previous section. The reason is that the resonance frequency of the quantum dots was chosen further from the band edge and the background loss was chosen higher than those for the thin coating. In Fig. 22 the normalized eigenmode for the second band at the  $X$  point is drawn for three different values of the pump  $\rho$ : exactly at threshold, just above threshold, and well above threshold. The normalized nonlinear Bloch waves do not exhibit significant difference from the normalized Bloch eigenmode of the backbone photonic crystal (BPC) at the same band and

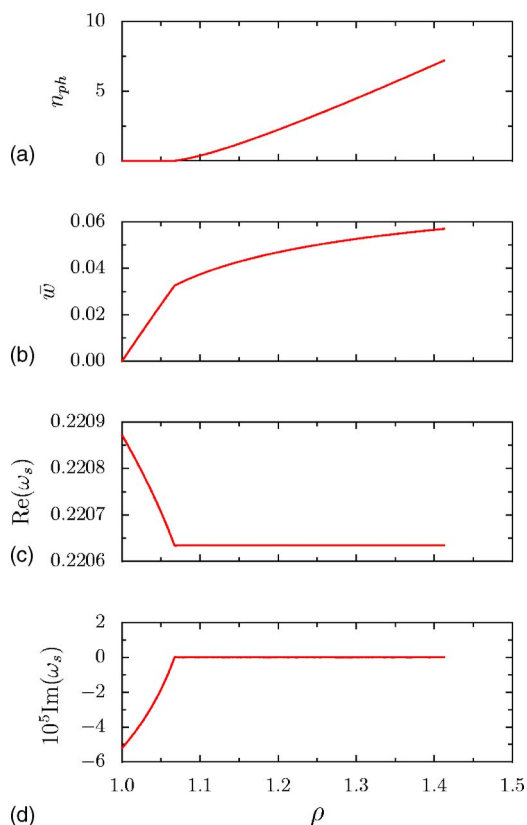


FIG. 21. (Color online) (a) The number of photons per unit cell  $n_{ph}$ , (b) average inversion  $\bar{w}$  of the dopant atoms, (c) the real part of the frequency of the second band at the  $X$  point, and (d) the imaginary part of the frequency of the second band at the  $X$  point—as functions of the pumping parameter  $\rho$ .

Bloch vector. However a plot of the absolute value of the difference of the normalized field with the BPC eigenmode reveals the modification of the eigenmode due to nonlinear interaction. As seen in Fig. 22, the mode structure modification is roughly 0.1% from that of the BPC. In Fig. 23, we

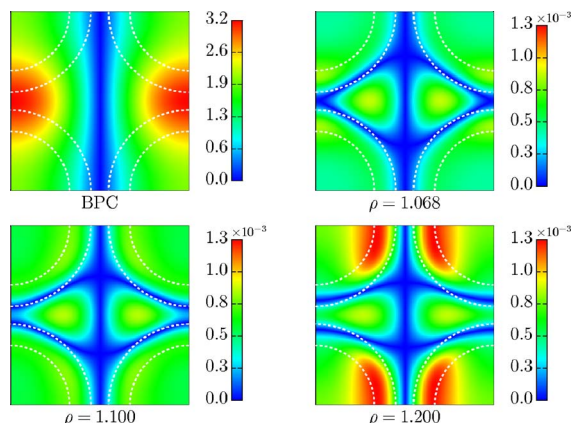


FIG. 22. (Color online) The absolute value of the difference of the normalized nonlinear Bloch field for  $\rho=1.068$  (upper right picture),  $\rho=1.1$  (lower left picture), and  $\rho=1.2$  (lower right picture) with the BPC eigenmode (upper left picture) has a small magnitude of the order of  $10^{-3}$ . The white dashed lines show the dielectric boundaries.

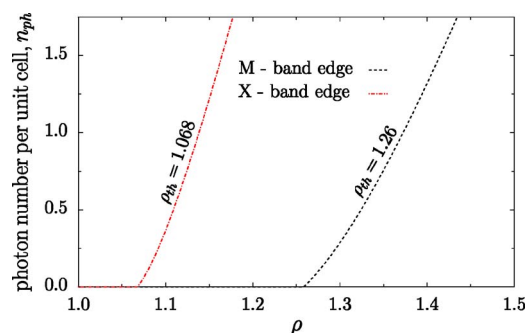


FIG. 23. (Color online) Transition threshold for the number of photons per unit cell,  $n_{ph}$ , occurs for a lower pump power at the upper band edge ( $X$  point).

plot the number of photons per unit cell,  $n_{ph}$ , in the self-consistent, nonlinear Bloch wave, near threshold for the two band edges, and for the loss given by Eq. (35). The resonance frequency of the quantum dots was placed exactly half way between  $X$  and  $M$  band edges. Clearly, the upper band edge exhibits a nonlinear Bloch wave for a lower pumping threshold than the lower band edge. In Fig. 24, we plot the growth of the photon number per unit cell in self-consistent nonlinear Bloch waves (with real eigenfrequency) for various choices of the background loss. As the loss is reduced, the threshold for steady state, nonlinear Bloch waves decreases, and the rate of increase of photon number per unit cell with pumping increases dramatically.

## VII. DISCUSSION

In this paper, we have demonstrated the existence of nonlinear waves, satisfying Bloch periodicity, with purely real eigenfrequency, in strong scattering photonic crystals exhibiting both loss and gain. We have delineated detailed characteristics of these modes for a model of rare-earth atoms doping of the solid region and for models of the colloidal quantum dot infiltration within the void regions of 2D PCs. Below a threshold pumping level of the two-level radiators, determined by the losses in the system, there are only transient extended modes in the photonic crystals. Localized or solitary wave solutions may nevertheless exist [57] under

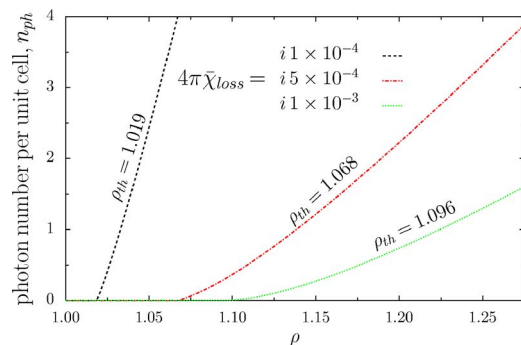


FIG. 24. (Color online) Dependency of the threshold for the pump parameter and the slope of the number of photons per unit cell versus the pump parameter, when the losses are varied.

suitable conditions and need to be investigated separately. Above the pumping threshold, nonlinear (extended) Bloch waves exist, analogous to Bloch modes in a linear photonic crystal. Unlike linear Bloch modes, the nonlinear Bloch waves are characterized by a specific amplitude (number of photons per unit cell) for each choice of the pump parameter. This nonlinear wave amplitude exhibits a laserlike input (pump)—output characteristics. Unlike band edge lasing observed in various photonic crystals [58], these nonlinear Bloch waves may occur throughout the spectrum of the photonic crystal and are not restricted to special spectral regions of vanishing photon group velocity. This suggests that, in general, losses in photonic crystals may be offset by the introduction of regions of gain to yield propagating as well as stationary Bloch waves throughout the photonic band structure. Although we have presented detailed results for only 2D bulk photonic crystals, similar nonlinear Bloch waves arise in 3D PBG systems and effectively 1D periodic systems. A particularly interesting example of the latter is a 1D waveguide embedded in a higher-dimensional photonic crystal. In this situation, losses within the waveguide may be compensated by incorporating active regions beside the waveguide. Likewise, our method may provide a more exact computational tool for describing laser activity in strongly scattering 1D distributed feedback lasers that have been traditionally [23,24] described by a more approximate set of coupled mode equations.

Our self-consistent iterative method for obtaining nonlinear Bloch wave solutions represents an important generalization of previously developed methods to treat photonic crystals with a frequency-dependent dielectric function. Our method enables the precise, quantitative treatment of strongly scattering PCs and PBG materials with a nonlinear and complex dielectric function. Two important extensions of the present work are the nonlinear media with an inhomogeneously broadened collection of resonators and to materials in which the dielectric constant is negative in some regions. For example, a metallic photonic crystal filament exhibiting quasithermal light emission [26,27] can be modeled as an inhomogeneously broadened collection of emitters with a very broad range of emitters. While such a medium exhibits very strong (blackbody) absorption loss, periodically structured metals may exhibit isolated pass bands [37], where light at frequencies below the bulk plasma cutoff frequency can propagate through a connected network of (air) holes. Modes within such pass bands may suffer minimal loss but at the same time can be excited by thermal emitters within the solid fraction of the filament. The excitation of nonlinear Bloch waves in such a pass band would have dramatic implications for quasithermal light emission when the system is driven slightly out of thermodynamic equilibrium. A second example where nonlinear Bloch waves might be generated is in materials with intrinsic loss. Here the incorporation of gain in specific parts of the unit cell can offset these losses. In left-handed metamaterials [59,60] both negative dielectric constant and negative magnetic permeability are present. When this is associated with a resonance, a significant imaginary part of the susceptibility appears, leading to losses. In the near-infrared spectrum, the best available materials [61] exhibit a ratio of real part to imaginary part of

the dielectric constant of order unity. It is, in principle, possible that the doping of such systems with gain material could offset these intrinsic losses. Here [61], the scale of periodicity is slightly below 400 nm for an operating wavelength of 1.4  $\mu\text{m}$ . It is possible that nonlinear Bloch waves could be generated, even at long wavelengths compared to the lattice constant, provided that the gain regions of each unit cell are pumped. The compensation of losses with gain and the emergence of undamped nonlinear Bloch waves may provide otherwise unattainable practical applications for a variety of materials of this nature.

#### ACKNOWLEDGMENT

This work was supported in part by the Natural Sciences and Engineering Research Council of Canada.

#### APPENDIX A: NORMALIZATION OF EIGENMODES FOR THE BACKBONE PHOTONIC CRYSTAL

In this Appendix we derive the normalization parameter  $\alpha_{\vec{k},l}$  for a Bloch mode of the backbone photonic crystal with Bloch wave vector  $\vec{k}$  and band index  $l$ . From Eq. (1) where we set  $\chi_{\omega}(\vec{r}) \equiv 0$ , and by using  $E_{\omega}(\vec{r}) = e^{i\vec{k}\vec{r}}u(\vec{r})$  with  $u(\vec{r}) = \sum_{\vec{G}} \tilde{u}(\vec{G}') e^{i\vec{G}'\vec{r}}$  a periodic function of the direct lattice (Bloch's theorem [5]) we obtain

$$\sum_{\vec{G}} \epsilon_{\vec{G}',\vec{G}}^{-1} (\vec{k} + \vec{G})^2 \tilde{u}(\vec{G}) = \frac{\omega^2}{c^2} \tilde{u}(\vec{G}'). \quad (\text{A1})$$

The solutions  $\{\psi_{\vec{k},l}(\vec{r})\}$  of the Hermitian equation [Eq. (A1)], corresponding to eigenvalues  $\{\omega_{\vec{k},l}\}$ , form a complete set of functions in the Hilbert space of Eq. (1).  $\psi_{\vec{k},l}(\vec{r}) = (e^{i\vec{k}\vec{r}}/\alpha_{\vec{k},l})u_{\vec{k},l}(\vec{r})$  and we choose the normalization constant  $\alpha_{\vec{k},l}$  of the Bloch function  $\psi_{\vec{k},l}(\vec{r})$  to be real and such that

$$\frac{1}{V_0} \int_{V_0} d^2r \psi_{\vec{k},l}^*(\vec{r}) \epsilon(\vec{r}) \psi_{\vec{k},l}(\vec{r}) = 1. \quad (\text{A2})$$

Using  $u_{\vec{k},l}(\vec{r}) = \sum_{\vec{G}'} \tilde{u}_{\vec{k},l}(\vec{G}') e^{i\vec{G}'\vec{r}}$  and  $\int_{V_0} d^2r e^{i\vec{G}\vec{r}} = V_0 \delta_{\vec{G},0}$  we obtain

$$\sum_{\vec{G}''} \tilde{u}_{\vec{k},l}^*(\vec{G}'') \left( \sum_{\vec{G}'} \epsilon_{\vec{G}'',\vec{G}'} \tilde{u}_{\vec{k},l}(\vec{G}') \right) = \alpha_{\vec{k},l}^2. \quad (\text{A3})$$

From Eq. (2) we can obtain

$$(\vec{k} + \vec{G}'')^2 \tilde{u}_{\vec{k},l}(\vec{G}'') = \frac{\omega_{\vec{k},l}^2}{c^2} \sum_{\vec{G}'} \epsilon_{\vec{G}'',\vec{G}'} \tilde{u}_{\vec{k},l}(\vec{G}'). \quad (\text{A4})$$

Inserting Eq. (A4) into Eq. (A3) we obtain

$$\alpha_{\vec{k},l} = \frac{\sqrt{\sum_{\vec{G}} |(\vec{k} + \vec{G}) \tilde{u}_{\vec{k},l}(\vec{G})|^2}}{\omega_{\vec{k},l}/c}. \quad (\text{A5})$$

#### APPENDIX B: ENERGY DENSITY AND PHOTON NUMBER IN FREQUENCY-DEPENDENT DIELECTRICS

In the case of dielectrics with frequency-dependent dielectric functions, absorption and/or dissipation of the elec-

tromagnetic field occurs. If the rate of absorption is small compared to the rate of oscillation of the electromagnetic field, the energy density of the electromagnetic field is well defined. The detailed relationship between this energy density and the field amplitudes, however, are modified by the frequency dependence of the dielectric function. This energy density is used in our method to determine the amplitude of the field under pumping conditions.

We start with Maxwell's equations

$$\vec{\nabla} \times \vec{E} = -\frac{1}{c} \frac{\partial \vec{H}}{\partial t}, \quad (\text{B1a})$$

$$\vec{\nabla} \times \vec{H} = \frac{4\pi}{c} \vec{j} + \frac{1}{c} \frac{\partial \vec{D}}{\partial t}. \quad (\text{B1b})$$

Dot multiplying Eq. (B1a) by  $\vec{H}$  and Eq. (B1b) by  $\vec{E}$  and then subtracting them side by side we obtain

$$-\vec{j} \cdot \vec{E} = \frac{1}{4\pi} \left[ \vec{E} \cdot \frac{\partial \vec{D}}{\partial t} + \vec{H} \cdot \frac{\partial \vec{H}}{\partial t} \right] + \vec{\nabla} \cdot \vec{S}, \quad (\text{B2})$$

where the Poynting vector is

$$\vec{S} = \frac{c}{4\pi} \vec{E} \times \vec{H}.$$

For a single free charge,  $\vec{j} \cdot \vec{E} = q\vec{v} \cdot \vec{E} = q\vec{E} \cdot d\vec{r}/dt = \vec{F} \cdot d\vec{r}/dt = dW/dt$  represents the rate of work that the field performs on the charge. In this view we may interpret Eq. (B2) as The work done by the free charge distribution on the field (left side of the equation) is partially stored as energy in the field (first term of the right side of the equation) and partially leaves the region as radiation (second term of the right side of the equation). Hence we may interpret  $1/4\pi[\vec{E} \cdot \partial \vec{D}/\partial t + \vec{H} \cdot \partial \vec{H}/\partial t]$  as the time rate of change of the energy density in the electromagnetic field. For a frequency-independent dielectric function the energy density  $U$  of the electromagnetic field is easily obtained

$$U = \frac{1}{8\pi} [\epsilon \vec{E}^2 + \vec{H}^2]. \quad (\text{B3})$$

For a frequency-dependent dielectric function  $\epsilon(\omega)$  the derivation of the energy density requires careful reconsideration. We write  $\epsilon(\omega) = \epsilon_R(\omega) + i\epsilon_I(\omega) = \epsilon^*(-\omega)$ , where  $\epsilon_R$  and  $\epsilon_I$  are the real and imaginary parts of the (bound charge) dielectric function, respectively, and the Fourier components of the time-dependent displacement and electric fields are related by  $\vec{D}_\omega = \epsilon(\omega) \vec{E}_\omega$ . In the presence of a free charge with non-zero conductivity ( $\sigma \neq 0$ ), the free current satisfies  $\vec{j} = \sigma \vec{E}$  (Ohm's law). From Eq. (B1b) we get for a single Fourier component

$$\vec{\nabla} \times \vec{H}_\omega \equiv \frac{-i\omega}{c} \bar{\epsilon}(\omega) \vec{E}_\omega,$$

where  $\bar{\epsilon}(\omega)$  is the total frequency-dependent dielectric function

$$\bar{\epsilon}(\omega) = \epsilon_R(\omega) + i \frac{4\pi\sigma + \omega\epsilon_I(\omega)}{\omega}.$$

We may interpret  $\sigma_b(\omega) \equiv \omega\epsilon_I(\omega)/4\pi$  as a bound charge conductivity that vanishes in the D.C. limit ( $\omega \rightarrow 0$ ), and

$$\vec{j}_b(t) \equiv \int_{-\infty}^{\infty} \sigma_b(\omega) \vec{E}_\omega e^{-i\omega t} d\omega,$$

may be called the bound current. In the case of absence of the free currents we rewrite Eq. (B2) as

$$-\vec{j}_b \cdot \vec{E} = \frac{1}{4\pi} \left[ \vec{E} \cdot \frac{\partial \vec{D}}{\partial t} + \vec{H} \cdot \frac{\partial \vec{H}}{\partial t} \right] + \vec{\nabla} \cdot \vec{S}, \quad (\text{B4})$$

where now

$$\vec{D}(t) = \int_{-\infty}^{\infty} \epsilon_R(\omega) \vec{E}(\omega) e^{-i\omega t} d\omega.$$

Then

$$\begin{aligned} \vec{E}(t) \frac{\partial \vec{D}(t)}{\partial t} &= \frac{1}{2} \frac{\partial}{\partial t} \int \int_{-\infty}^{\infty} \vec{E}(-\omega') \vec{E}(\omega) \frac{\omega \epsilon_R(\omega) - \omega' \epsilon_R(\omega')}{\omega - \omega'} \\ &\quad \times e^{-i(\omega - \omega')t} d\omega' d\omega. \end{aligned} \quad (\text{B5})$$

Let us suppose that the electric field  $\vec{E}(t)$  is quasimonochromatic, namely  $\vec{E}(\omega) \neq 0$  only for a small region of frequencies about some carrier frequency  $\omega_0$ . This means that the field  $\vec{E}(t)$  oscillates with frequency  $\omega_0$  and changes its amplitude in a time scale much longer than  $T = 2\pi/\omega_0$ . We introduce  $\omega = \omega_0 + \alpha$  and  $\omega' = \omega_0 + \beta$  to obtain this contribution, about  $\omega_0$

$$\lim_{\alpha, \beta \rightarrow 0} \frac{\omega \epsilon_R(\omega) - \omega' \epsilon_R(\omega')}{\omega - \omega'} \simeq \left. \frac{\partial [\omega \epsilon_R(\omega)]}{\partial \omega} \right|_{\omega_0}.$$

Hence

$$\vec{E}(t) \frac{\partial \vec{D}(t)}{\partial t} \simeq \frac{1}{2} \left. \frac{\partial [\omega \epsilon_R(\omega)]}{\partial \omega} \right|_{\omega_0} \frac{\partial \vec{E}^2(t)}{\partial t}. \quad (\text{B6})$$

This approximation may break down in situations where the imaginary part of the dielectric constant and the corresponding frequency derivative of  $\epsilon_R(\omega)$  is too large. In this case the field is not sufficiently monochromatic and we must retain the detailed expression [Eq. (B5)]. Substitution of Eq. (B6) into Eq. (B4) gives  $-\vec{j}_b \cdot \vec{E} \equiv \partial U/\partial t + \vec{\nabla} \cdot \vec{S}$  where

$$U = \frac{1}{8\pi} \left[ \left. \frac{\partial [\omega \epsilon_R(\omega)]}{\partial \omega} \right|_{\omega_0} \vec{E}^2 + \vec{H}^2 \right] \quad (\text{B7})$$

is the energy density of a quasi-monochromatic electromagnetic field.

For the case of frequency-independent dielectric constant it is straightforward to show that

$$b \int_{V_0} d^2r \overline{U_E(\vec{r}, t)} = \hbar \omega n_{ph}, \quad (\text{B8})$$

where  $V_0$  is the volume of the two-dimensional unit cell of the photonic crystal,  $\overline{U_E(\vec{r}, t)} = \epsilon/8\pi E^2(\vec{r}, t)$  is the cycle averaged electric field energy density, and  $n_{ph}$  is the number of photons per two-dimensional unit cell  $V_0$ , per unit height  $b$ . We assume that the same expression applies to a frequency-dependent dielectric function with the modified electric field energy density appearing in Eq. (B6).

### APPENDIX C: OPTICAL SUSCEPTIBILITY MODEL FOR $\text{Er}^{3+}$ IN GLASS

#### 1. Dipole moment and relaxation times of transition for erbium in glass matrix

The  $\text{Er}^{3+}$  laser transition has a wavelength  $\lambda_0 = 1535.8$  nm ( $\nu_0 = 1.95 \times 10^{14}$  Hz) [62]. The dipole moment of the transition defined as  $d = ez_{21} = e\langle 1|z|2\rangle$  is related to the transition oscillator strength  $f \cong 8.21 \times 10^{-7}$  ([47], p. 198) by

$$d = (ez_{21}) = \left( \frac{e^2 \hbar}{2m\omega_0} f \right)^{1/2} \cong 3.15 \times 10^{-32} \text{C m}.$$

The coefficient of spontaneous emission (*radiative decay*) of erbium ions implanted into a glass ( $\text{SiO}_2$ ) matrix ( $\epsilon_b = 2.1$ ) is given by [63]

$$A_{21} = \sqrt{\epsilon_b} \frac{d^2 \omega_0^3}{3\pi\epsilon_0 \hbar c^3} \cong 11.2 \text{ Hz}.$$

The longitudinal time  $T_1$  of the susceptibility (*depopulation time* of level  $|2\rangle$  toward other levels ([47], p. 249) is the sum of spontaneous emission and nonradiative emission rates

$$\frac{1}{T_1} = A_{21} + \Gamma_{21}. \quad (\text{C1})$$

From experiments  $T_1 \cong 14.4$  ms suggesting that the decay rate of the upper laser level  $|2\rangle$  to lower level  $|1\rangle$  due to *nonradiative* relaxation processes is  $\Gamma_{21} \cong 58$  Hz. On the other side the laser transition of erbium has a Lorentzian line shape (elastic collisions) of width (FWHM)

$$\delta\nu_0 \cong 1.8 \times 10^{11} \text{ Hz}.$$

Since the depopulation time is extremely slow, this linewidth can be interpreted as the dipole dephasing time scale  $T_2 \cong (\delta\nu_0)^{-1} \cong 5.6$  ps.

#### 2. Parameters for the susceptibility of dopant atoms in photonic crystal

The scaled frequencies of the photonic crystal are defined as  $\omega_s = \omega a / 2\pi c = a/\lambda$  (where  $a$  is the lattice constant of the photonic crystal) and  $\omega_{0s} = a/\lambda_0$ . For  $T_1 = 14.4$  ms and  $T_2 = 5.6$  ps the scaled depopulation time is  $\tau_1 = 2\pi c/aT_1 = 2\pi c/\omega_{0s}\lambda_0 T_1 = 1.77/\omega_{0s} \times 10^{13}$  and the scaled dephasing time is  $\tau_2 \cong 2\pi c/aT_2 = 2\pi c/\omega_{0s}\lambda_0 T_2 = 6.82/\omega_{0s} \times 10^3$ , where we used  $\lambda_0 = 1535.8$  nm. For an atomic density  $N_T = 10^{19} \text{ cm}^{-3}$  and the parameters  $d$  and  $T_2$ , described above,

the susceptibility strength parameter [Eq. (18b)] is

$$g_0 \cong 5.92 \times 10^{-5} \frac{\rho - 1}{\rho + 1}. \quad (\text{C2})$$

The FWHM of the amplifying part of the susceptibility of the dopant atoms, for very weak electric fields [Eq. (19)] is  $\delta\omega_{0s} = 2/\tau_2 = 2.93 \times 10^{-4} \omega_{0s}$ . If we wish to place the emission line  $\lambda_0$  of the dopant atoms within one FWHM away from the  $X$ -point band edge at  $\omega_s = 0.266401$ , we require  $\omega_{0s} = 0.266323$ . This corresponds to a photonic crystal lattice constant of  $a = \omega_{0s}\lambda_0 = 409$  nm. Erbium ions may be optically pumped at a wavelength of  $\lambda_p = 1480$  nm corresponding to a scaled frequency of  $\omega_{ps} = 0.276364$ . The position- and frequency-dependent intensity of the mode function defined in Eq. (30) becomes with the help of the above parameters and  $b = a$ ,  $\lambda_0 = 1535.8$  nm

$$I_{\omega_s}(\vec{r}) = n_{ph} \frac{1.16}{\omega_{0s}^3 (\rho + 1)} |\psi_{\vec{q}}(\vec{r})|^2. \quad (\text{C3})$$

#### 3. Normalization of the spatial part of the electric field

Normalization of the spatial part  $\psi(\vec{r})$  of the electric field is done according to Eq. (28). The total dielectric constant of the doped photonic crystal is

$$\epsilon(\vec{r}, \omega) = \epsilon_{\text{BPC}}(\vec{r}) + 4\pi\bar{\chi}(\vec{r}, \omega) + 4\pi\bar{\chi}_{\text{loss}}(\vec{r}). \quad (\text{C4})$$

In our calculations, we use the expression

$$\begin{aligned} & \frac{\partial[\omega\epsilon_{\text{R}}(\omega)]}{\partial\omega} \\ &= \epsilon_{\text{R}}(\vec{r}, \omega_s) + \frac{4\pi g_0 \omega_s \tau_2 [1 - (\omega_s - \omega_{0s})^2 \tau_2^2 + I_{\omega_s}(\vec{r})] \theta_a(\vec{r})}{[1 + (\omega_s - \omega_{0s})^2 \tau_2^2 + I_{\omega_s}(\vec{r}) \omega_s \omega_{0s}^{-1}]^2} \end{aligned} \quad (\text{C5})$$

where, for simplicity,  $\partial|\psi(\vec{r})|^2/\partial\omega_s$  is discarded.

### APPENDIX D: SUSCEPTIBILITY PARAMETERS FOR COLLOIDAL QUANTUM DOTS

We assume that the resonance frequency of the colloidal quantum dots corresponds to a wavelength  $\lambda_0 = 1.55 \mu\text{m}$ . To place the resonance frequency of the quantum dots at a scaled frequency  $\omega_{0s}$ , a lattice constant  $a = \omega_{0s}\lambda_0$  is necessary. A radius  $r = 4.5$  nm for the capped (semiconductor-core radius 2.5 nm) colloidal quantum dots gives a volumetric concentration  $N_T = \sqrt{2}/16r^3 \cong 9.7 \times 10^{17} \text{ cm}^{-3}$  if they are fcc close packed. We assume a dipole moment for the resonant transition  $d \cong 2 \times 10^{-29} \text{ C m}$  [11,64]. In addition we assume a population decay time  $T_1 \cong 1$  ns [65] giving  $\tau_1 \cong 5.1 \times 10^6$ , and a dephasing time  $T_2 \cong 1$  ps giving  $\tau_2 \cong 5.1 \times 10^3$ . The magnitude of the frequency-dependent part of the susceptibility of the quantum dots is [Eq. (18b)]

$$g_0 = 0.44 \frac{\rho - 1}{\rho + 1}. \quad (\text{D1})$$

The FWHM of the amplifying part of the susceptibility of the dopant atoms, for very weak electric fields [Eq. (19)], is

$\delta\omega_{0s}=2/\tau_2=4\times 10^{-4}$ . This corresponds to a linewidth of  $\delta\lambda\approx 0.0026\ \mu\text{m}$  centered at  $\lambda_0=1.55\ \mu\text{m}$  and  $\delta\lambda/\lambda_0\approx 0.17\%$  homogeneous line broadening for quantum dots.

The position- and frequency-dependent intensity of the mode function defined in Eq. (30) (using  $d=2\times 10^{-29}\ \text{C m}$ ,

$T_1=1\ \text{ns}$ ,  $T_2=1\ \text{ps}$ ,  $b=a$ ,  $a=\omega_{0s}\lambda_0$ , and  $\lambda_0=1.55\ \mu\text{m}$ ) is

$$I_{\omega_s}(\vec{r}) = n_{ph} \frac{1.76 \times 10^{-2}}{\omega_{0s}^3(\rho + 1)} |\psi_{\vec{q}}(\vec{r})|^2. \quad (\text{D2})$$

- 
- [1] S. John, Phys. Rev. Lett. **58**, 2486 (1987).  
 [2] E. Yablonovitch, Phys. Rev. Lett. **58**, 2059 (1987).  
 [3] S. John, Phys. Rev. Lett. **53**, 2169 (1984).  
 [4] N. W. Ashcroft and N. D. Mermin, *Solid State Physics* (Saunders College Publishing, 1976).  
 [5] K. M. Ho, C. T. Chan, and C. M. Soukoulis, Phys. Rev. Lett. **65**, 3152 (1990).  
 [6] P. Lodahl, A. Floris van Driel, I. S. Nikolaev, A. Irman, K. Overgaag, D. Vanmaekelbergh, and W. L. Vos, Nature (London) **430**, 654 (2004).  
 [7] T. Yoshie, A. Scherer, J. Hendrickson, G. Khitrova, H. M. Gibbs, G. Rupper, C. Ell, O. B. Shchekin, and D. G. Deppe, Nature (London) **432**, 203 (2004).  
 [8] J. I. Fushman and D. Englund, Appl. Phys. Lett. **87**, 241102 (2005).  
 [9] K. Kounoike, M. Yamauchi, M. Fujita, T. Asano, J. Nakanishi, and S. Noda, Electron. Lett. **41**, 1402 (2005).  
 [10] M. Shib and P. Guyot-Sionnest, J. Chem. Phys. **111**, 6955 (1999).  
 [11] K. L. Silverman, R. P. Mirin, S. T. Cundiff, and A. G. Norman, Appl. Phys. Lett. **82**, 4552 (2003).  
 [12] S. G. Cloutier, P. A. Kossyrev, and J. Xu, Nat. Mater. **4**, 891 (2005).  
 [13] O. Painter, R. K. Lee, A. Scherer, A. Yariv, J. D. O'Brien, P. D. Dapkus, and I. Kim, Science **284**, 1819 (1999).  
 [14] H. G. Park, S. H. Kim, S. H. Kwon, Y. G. Ju, J. K. Yang, J. H. Baek, S. B. Kim, and Y. H. Lee, Science **305**, 1444 (2004).  
 [15] S. Strauf, K. Hennessy, M. T. Rakher, Y. S. Choi, A. Badolato, L. C. Andreani, E. L. Hu, P. M. Petroff, and D. Bouwmeester, Phys. Rev. Lett. **96**, 127404 (2006).  
 [16] M. Kim, C. S. Kim, W. W. Bewley, J. R. Lindle, C. L. Canedy, I. Vurgaftman, and J. R. Meyer, Appl. Phys. Lett. **88**, 191105 (2006).  
 [17] A. M. Yacomotti, F. Raineri, G. Vecchi, P. Monnier, R. Raj, A. Levenson, B. BenBakir, C. Seassal, X. Letartre, and P. Viktorovitch, Appl. Phys. Lett. **88**, 231107 (2006).  
 [18] N. Hitoshi, Y. Sugimoto, K. Kanamoto, N. Ikeda, Y. Tanaka, Y. Nakamura, S. Ohkouchi, Y. Watanabe, K. Inoue, and H. Ishikawa, Opt. Express **12**, 6606 (2004).  
 [19] D. Vujic and S. John, Phys. Rev. A **72**, 013807 (2005).  
 [20] S. Noda, M. Yokoyama, M. Imada, A. Chutinan, and M. Mochizuki, Science **293**, 1123 (2001).  
 [21] K. Sakoda, K. Ohtaka, and T. Ueta, Opt. Express **4**, 481 (1999).  
 [22] S. Nojima, Science **37**, L565 (1998).  
 [23] A. Yariv and P. Yeh, *Optical Waves in Crystals* (John Wiley & Sons, New York, 1984).  
 [24] H. Kogelnik and C. V. Shank, J. Appl. Phys. **43**, 2327 (1972).  
 [25] J. G. Fleming, S. Y. Lin, I. El-Kady, R. Biswas, and K. M. Ho, Nature (London) **417**, 52 (2002).  
 [26] S. Y. Lin, J. Moreno, and J. G. Fleming, Appl. Phys. Lett. **83**, 380 (2003).  
 [27] S. Y. Lin, J. Moreno, and J. G. Fleming, Opt. Lett. **28**, 1909 (2003).  
 [28] C. H. Seager, M. B. Sinclair, and J. G. Fleming, Appl. Phys. Lett. **86**, 244105 (2005).  
 [29] I. El-Kady, W. W. Chow, and J. G. Fleming, Phys. Rev. B **72**, 195110 (2005).  
 [30] A. R. McGurn and A. A. Maradudin, Phys. Rev. B **48**, 17576 (1993).  
 [31] V. Kuzmiak, A. A. Maradudin, and F. Pincemin, Phys. Rev. B **50**, 16835 (1994).  
 [32] V. Kuzmiak and A. A. Maradudin, Phys. Rev. B **55**, 7427 (1997).  
 [33] V. Kuzmiak and A. A. Maradudin, Phys. Rev. B **58**, 7230 (1998).  
 [34] K. Sakoda and J. Kawamata, Opt. Express **3**, 12 (1998).  
 [35] K. Sakoda, N. Kawai, T. Ito, A. Chutinan, S. Noda, T. Mitsuyu, and K. Hirao, Phys. Rev. B **64**, 045116 (2001).  
 [36] T. Ito and K. Sakoda, Phys. Rev. B **64**, 045117 (2001).  
 [37] O. Toader and S. John, Phys. Rev. E **70**, 046605 (2004).  
 [38] V. P. Bykov, Sov. J. Quantum Electron. **4**, 861 (1975).  
 [39] S. John and J. Wang, Phys. Rev. Lett. **64**, 2418 (1990).  
 [40] S. John and J. Wang, Phys. Rev. B **43**, 12772 (1991).  
 [41] S. John and T. Quang, Phys. Rev. A **50**, 1764 (1994).  
 [42] E. Yablonovitch, J. Opt. Soc. Am. B **10**, 283 (1993).  
 [43] S. John and T. Quang, Phys. Rev. Lett. **76**, 2484 (1996).  
 [44] T. Quang and S. John, Phys. Rev. Lett. **78**, 1888 (1997).  
 [45] S. John and T. Quang, Phys. Rev. A **56**, 4273 (1997).  
 [46] K. Busch and S. John, Phys. Rev. E **58**, 3896 (1998).  
 [47] P. W. Milonni and J. H. Eberly, *Lasers* (John Wiley & Sons, New York, 1988).  
 [48] A. E. Siegman, *Lasers* (University Science Books, 1986).  
 [49] K. Sakoda, *Optical Properties of Photonic Crystals*, Springer series in Optical Sciences (Springer-Verlag, Berlin, 2001).  
 [50] A. R. McGurn, Phys. Rev. B **53**, 7059 (1996).  
 [51] K. Gottfried and T. M. Yan, *Quantum Mechanics: Fundamentals*, 2nd ed. (Springer, New York, 2003).  
 [52] A. Yariv, *Introduction to Theory and Applications of Quantum Mechanics* (John Wiley & Sons, New York, 1982).  
 [53] M. Florescu and S. John, Phys. Rev. A **64**, 033801 (2001).  
 [54] N. Vats and S. John, Phys. Rev. A **58**, 4168 (1998).  
 [55] F. W. Wise, Acc. Chem. Res. **33**, 773 (2000).  
 [56] V. I. Klimov, J. Phys. Chem. B **104**, 6112 (2000).  
 [57] N. Aközbebek and S. John, Phys. Rev. E **58**, 3876 (1998).  
 [58] V. I. Kopp, B. Fan, H. K. Vithana, and A. Z. Genack, Opt. Lett. **23**, 1707 (1998).  
 [59] V. G. Veselago, Sov. Phys. Usp. **10**, 509 (1968).  
 [60] D. R. Smith, J. B. Pendry, and M. C. K. Wiltshire, Science **305**, 788 (2004).

- [61] C. Enkrich, M. Wegener, S. Linden, S. Burger, L. Zschiedrich, F. Schmidt, J. F. Zhou, Th. Koschny, and C. M. Soukoulis, *Phys. Rev. Lett.* **95**, 203901 (2005).
- [62] W. J. Miniscalco, *J. Lightwave Technol.* **9**, 234 (1991).
- [63] S. M. Barnett, B. Huttner, R. Loudon, and R. Matloob, *J. Phys. B* **29**, 3763 (1996).
- [64] P. G. Eliseev, H. Li, A. Stintz, G. T. Liu, T. C. Newell, K. J. Malloy, and L. F. Lester, *Appl. Phys. Lett.* **77**, 262 (2000).
- [65] C. H. Henry and K. Nassau, *Phys. Rev. B* **1**, 1628 (1970).